Journal of Hydrology 659 (2025) 133309

Contents lists available at ScienceDirect

Journal of Hydrology

journal homepage: www.elsevier.com/locate/jhydrol

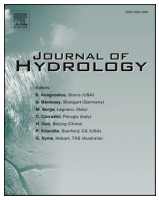

Research papers

Global droughts in a warming climate: Evaluation of SPI and SPEI under 1.5°, 2°, and 3 °C global warming

Kunal Bhardwaj [a], Ashok Mishra [a,b], C. Prakash Khedun [c,*]

[a] Glenn Department of Civil Engineering, Clemson University, Clemson, SC 29634, United States
[b] Zachry Department of Civil and Environmental Engineering, Texas A&M University, College Station, TX 77843, United States
[c] Department of Agricultural Sciences/S.C. Water Resources Center, Clemson University, Pendleton, SC 29670, United States

ARTICLE INFO

Keywords:
CMIP6
Drought
SPI
SPEI

ABSTRACT

Accurately predicting droughts, amidst rapid global warming, is crucial for effective resource management and policy development. Here, we employ CMIP6 models to analyze historical and future global meteorological drought patterns using the Standardized Precipitation Index (SPI) and Standardized Precipitation and Evapotranspiration Index (SPEI). We first assess model efficacy against historical observations (1951–2014) and then project changes at key IPCC warming thresholds. Our evaluation shows that even though CMIP6 models accurately capture global average drought characteristics, significant biases emerge in regions that commonly experience extreme historical drought conditions. Projections indicate increasing drought duration, frequency, and severity, particularly under higher warming scenarios. A more pronounced increase is noted with SPEI compared to SPI: under a 3 °C warming, drought severity is projected to increase across 91.8 % of land grids, based on SPEI, as opposed to 28.2 % for SPI. Similarly, increases in drought frequency are projected over 86.5 % (SPEI) versus 33.4 % (SPI), and increases in duration in 74.9 % (SPEI) versus 12.9 % (SPI) of land grids. This discrepancy highlights the importance of including temperature, through evapotranspiration, in drought assessments, especially because of the expected increase in evaporative demand driven by rising temperature. Our analysis further demonstrates that whereas humid and transitional areas may experience reduced drought severity and duration as per SPI, SPEI predicts a significant worsening of drought events in the future. On the other hand, both indicators project a worsening of drought conditions in arid regions—changes in SPI are small but that with SPEI are in the order of 2–3 months in duration, 3.5–4 events in frequency, and 4.3–5.2 units in severity. This study underscores the complexity of future drought patterns, which necessitates a range of strategies for mitigation and adaptation to safeguard against escalating drought risks in a warming world.

1. Introduction

Droughts are a recurrent natural hazard marked by significant dryness and water scarcity. Several regions around the world have been recurrently exposed to devastating droughts driven by precipitation deficits and extreme dryness leading to crop failures and wildfires (Richardson et al., 2022; Taufik et al., 2017). From 1981 to 2020, droughts repeatedly caused significant damages worldwide, with economic losses estimated between 6 and 8 billion USD in the United States (US) and Europe alone (Naumann et al., 2021; Smith, 2020). A changing climate introduces more uncertainty on droughts worldwide. Climate model projections are becoming increasingly important in planning and mitigation, provided that they can accurately represent observed hydrometeorological anomalies (Khedun & Singh, 2014; Singh et al., 2014).

Global Climate Models (GCMs) are advanced physics-based tools designed to study Earth system's responses to natural climate variability and human-induced increases in greenhouse gas emissions, often represented through corresponding changes in radiative forcing. Through a globally coordinated effort, the Coupled Model Intercomparison Project (CMIP) offers a comprehensive collection of GCM simulations by employing a standardized set of future radiative pathways, such as those mentioned in IPCC assessments for highlighting future climate changes and their implications (Eyring et al., 2016; IPCC, 2021). The recently released CMIP6 collection offers more GCM ensemble simulations, with improved representation of Earth's various atmospheric, land, and

* Corresponding author.
E-mail addresses: pkhedun@clemson.edu, pkhedun@gmail.com (C.P. Khedun).

https://doi.org/10.1016/j.jhydrol.2025.133309
Received 26 January 2025; Received in revised form 9 April 2025; Accepted 11 April 2025
Available online 14 April 2025

coupled processes (Eyring et al., 2016). Whereas GCM simulations have been shown to capture overall trends in dryness and water availability over an observed historical period, regional areas of high bias from observations may persist (Cook et al., 2020; Ukkola et al., 2020; Wang et al.,2021; Zhao and Dai, 2022). Additionally, due to inherent differences in model structures and parameterizations, simulated outputs of various GCMs are significantly different from each other (Nasrollahi et al., 2015; Ukkola et al., 2018, 2020; Vicente-Serrano et al., 2022; Zhao & Dai, 2017). As intermodal differences remain the largest source of uncertainty regarding future drought changes, understanding how well GCMs align during historical periods is vital for identifying weaknesses in future drought simulations (Burke & Brown, 2008; Swann et al., 2016; Zhao & Dai, 2015). Although CMIP6 models have enhanced abilities to simulate long-term precipitation trends in specific regions, assessing their accuracy in historical drought detection remains to be explored (Gusain et al., 2020; Peña-Angulo et al., 2020; Rivera and Arnould, 2020).

Droughts are known for their multifaceted impacts, as moisture deficit affects vegetation, water availability, and other interconnected socio-economic systems. A deficient rainfall combined with increased evaporation from the land surface typically initiates a drought's impact on a region's hydrological cycle (Gimeno-Sotelo et al., 2024; Mishra and Singh, 2010). Hence, variations of these meteorological conditions from their long-term "normal" indicate drought periods, called meteorological drought. They are monitored using indicators such as the Standardized Precipitation Index (SPI) and the Standardized Precipitation Evapotranspiration Index (SPEI). Incorporating evapotranspiration in SPEI makes it sensitive to local aerodynamic and radiative responses and more reflective of plant stresses (Vicente-Serrano et al., 2010, 2020). Unlike aridity, which defines long-term climatic water balance, drought is a temporary aberration common to most places on Earth. However, the interactions of various aerodynamic and land processes, which are different over different regions, determine how quickly drought conditions develop, whether the climatic balance allows some deficits to be attenuated, and how well natural and human populations are adapted against adverse impacts of droughts (AghaKouchak et al., 2021; Mishra and Singh, 2010; Mukherjee et al., 2018; Spinoni et al., 2021; Vicente-Serrano et al., 2020 ; Wada et al., 2013; Wu et al., 2024; Yang et al., 2016).

The number and duration of droughts have increased by 29 %, since 2000; a number of which are linked to global warming and its disruption of local weather patterns leading to an increase in drought risks in regions such as North America, Europe, South Africa, and Asia (Diffenbaugh et al., 2015; Mishra et al., 2021; Mukherjee and Mishra, 2021; Otto et al., 2018; UNCCD: Drought in Numbers, 2022; Williams et al., 2015;). In this context, the warming targets established in the Paris Climate Agreement have become key focal points in global studies on drought (Lehner et al., 2017; Wu et al., 2022; Xu et al., 2019). Drought projections at different warming thresholds, such as 1.5 °C, 2 °C, and 3 °C, provide vital information for policymaking and for adaptation efforts to mitigate future drought risks (IPCC, 2021; Wilhite et al., 2014). Furthermore, understanding the impacts of drought at various warming levels is crucial for physical systems, such as glaciers and biodiversity, which are likely to experience abrupt and significant challenges as temperatures rises (Lenton and Ciscar, 2013; Ritchie et al., 2021).

In this study, we first assess CMIP6 models' performance in reproducing observed meteorological droughts before assessing global drought changes in future warming periods. The effects of a drought event can be quantified in terms of its duration, severity, and frequency, building up as components of drought risk. Several studies have assessed changes in drought conditions by evaluating changes in drought characteristics from the observed historical to future periods under various emission scenarios (Chiang et al., 2021; Naumann et al., 2021; Spinoni et al., 2014, 2019). In our study, meteorological droughts are simulated using the output variables from the historical (1950–2014) and future (2015–2100) simulations of CMIP6 GCMs. We first assess the global performance of GCM outputs for simulating historical droughts by comparing the average historical drought characteristics obtained from GCMs against those obtained from a reference dataset. Next, we utilize the models' future simulations to project changes in meteorological drought characteristics from a recent reference period to future 30-year periods when the global mean surface temperature has risen by 1.5°, 2°, and 3 °C, as per IPCC assessments (IPCC, 2022). Furthermore, we present the aggregate shifts in drought characteristics across different aridity regions. Beyond variations in mean climate, differences in vegetation, topography, and population density may necessitate tailored approaches to mitigate the increasing risk of drought. Therefore, in this study, we address the following questions:

1. How accurately do CMIP6 models simulate meteorological droughts compared to observed data?
2. What are the projected changes in meteorological drought characteristics at different levels of global warming (1.5°, 2°, and 3 °C) from CMIP6 models?
3. How are current aridity zones projected to face changes in droughts?

By addressing these questions, we seek to enhance the understanding of model capabilities and limitations in simulating and projecting droughts, thereby contributing to more effective drought risk management and mitigation strategies under a warming climate.

2. Data and methodology

2.1. Simulated and reference dataset

Meteorological drought assessment necessitates the quantification of both precipitation deficits and atmospheric water demand, typically represented by potential evapotranspiration (PET). Whereas precipitation is directly available from CMIP GCM outputs, evapotranspiration is usually computed offline and is often derived from the aerodynamic and radiative components controlling it. Therefore, for this study, the first ensemble outputs (r1i1p1f1) of eight CMIP6 GCMs having datasets of precipitation (pr), surface temperature (tasmin, tasmax), wind speeds (uas, vas), surface air pressure (ps), surface relative humidity (hurs), and net incoming solar radiation (rsds, rlds), at a monthly resolution and spatial resolutions ranging from 0.9375° to 2.8° were selected and downloaded from the CMIP6 archive (Table 1; https://esgf-node.llnl.gov/projects/cmip6/). Whereas CMIP5 outputs are based on stabilized radiative forcings (RCPs) by the end of the 21st century, CMIP6 combines Shared Socio-economic Pathways (SSPs) with RCPs to account for socio-economic developments affecting greenhouse gas emissions (Riahi

Table 1
List of CMIP6 models.

Model no.	GCM Name	Variant	Original Resolution (Lat × Lon)	Key Reference
1	ACCESS-CM2	r1i1p1f1	1.25° × 1.875°	Bi et al. (2020)
2	ACCESS-ESM1-5	r1i1p1f1	1.25° × 1.875°	Ziehn et al. (2020)
3	CanESM5	r1i1p1f1	2.8° × 2.8°	Swart et al. (2019)
4	GFDL-ESM4	r1i1p1f1	1° × 1°	Dunne et al. (2020)
5	MIROC6	r1i1p1f1	1.4° × 1.4°	Tatebe et al. (2019)
6	MPI-ESM1-2-HR	r1i1p1f1	0.9375° × 0.9375°	Müller et al. (2018)
7	MPI-ESM1-2-LR	r1i1p1f1	1.875° × 1.875°	Mauritsen et al. (2019)
8	MRI-ESM2-0	r1i1p1f1	1.125° × 1.125°	Yukimoto et al. (2019)

et al., 2017). Two future scenarios were selected to represent contrasting pathways: SSP2-4.5, a "middle-of-the-road" scenario with moderate mitigation challenges, leading to 4.5 W/m^2 radiative forcing by 2100, and SSP5-8.5, a "high-end" scenario with rapid economic growth and high energy use, resulting in 8.5 W/m^2 radiative forcing by 2100. These scenarios capture a range of potential futures, as highlighted in IPCC assessments, and provide insights into drought impacts under varying global warming levels.

Although some studies use bias correction techniques to align model-simulated precipitation and evapotranspiration with historical observations, many large-scale investigations of drought and other climate extremes rely on raw GCM outputs (Almazroui et al., 2021; Al-Yaari et al., 2023; Bjarke et al., 2024; Christian et al., 2023; Dai & Zhao, 2017; Liu et al., 2018; Norris et al., 2022; Wang et al., 2021; Zhao & Dai, 2022). Bias correction can disrupt the physical consistency among GCM-simulated variables, especially in processes involving both evapotranspiration and soil moisture (Al-Yaari et al., 2023; Maraun, 2016). Moreover, it may not reliably correct future extremes or trends, often assuming stationarity and potentially yielding erroneous results. Lastly, the effectiveness of bias correction depends heavily on data availability and regional characteristics and can fail in data-sparse or topographically complex areas (Chen et al., 2013, 2020; Michalek et al., 2024). Although bias correction can address certain GCM biases in simulated variables, it does not necessarily improve drought detection (Papalexiou et al., 2021). Therefore, we use climate model outputs to generate drought variables and indices, enabling a global assessment of inherent GCM limitations without additional uncertainties from bias correction.

We used the University of East Anglia Climate Research Unit's TS4.0 (CRU TS) monthly gridded dataset (Harris et al., 2020) to benchmark the performance of selected CMIP6 model outputs. This dataset leverages records from an extensive network of ground-based stations and apply interpolation techniques to provide gridded observations at a 0.5° resolution. These datasets encompass primary variables (predominantly observed, such as precipitation and temperature), secondary variables (e.g., cloud cover and vapor pressure), and tertiary variables (e.g., potential evapotranspiration derived through applied methodologies).

The CRU dataset's extensive applications and rigorous quality control makes it a trusted resource for various climate assessments, including numerous drought studies (Papalexiou et al., 2021; Ridder et al., 2021; Spinoni et al., 2019; Ukkola et al., 2018). We used precipitation and potential evapotranspiration to identify observed droughts during the historical period spanning 1950 to 2014.

2.2. Potential evapotranspiration

Potential Evapotranspiration (PET) quantifies atmospheric water demand which influences soil desiccation and plant stress (Vicente-Serrano et al., 2020). Since PET is not directly available from GCM outputs, it is often computed offline through different methods. We used the Food and Agriculture Organization's recommended FAO-56 Penman-Monteith method to estimate monthly PET (reference crop PET; Allen et al., 1998). Penman-Montieth method incorporates a comprehensive set of climatic variables, including temperature, wind speed, solar radiation, and relative humidity, and provides more accurate and reliable estimates of PET than methods based on temperature and latitude, which have been shown to exaggerate future droughts (Aadhar and Mishra, 2020; Milly and Dunne, 2016).

The FAO-56 Penman-Monteith equation used for calculating PET (mm/day) is given by:

$$PET = \frac{0.408\Delta(R_n - G) + \gamma \frac{900}{T+273} u_2 (e_s - e_a)}{\Delta + \gamma(1 + 0.34u_2)} \quad (1)$$

where Δ is the slope of the vapor pressure curve at a given temperature (kPa °C^{-1}), R_n represents net radiation (M.J. m^{-2} day^{-1}), G is the soil heat flux density (M.J. m^{-2} day^{-1}), γ is the psychrometric constant (kPa °C^{-1}), T is the mean daily temperature (°C), u_2 is the wind speed at 2 m (m s^{-1}), and $e_s - e_a$ represents the saturation vapor pressure deficit (kPa).

We employed the mean monthly GCM outputs of temperature, wind, surface pressure, relative humidity, and net solar radiation to find the monthly PET for each model in historical and future SSP scenarios (Gu et al., 2020). Additionally, the reference dataset (CRU TS) also utilizes the Penman-Monteith method to provide PET outputs for the historical period.

2.3. Drought Indices: SPI and SPEI

We evaluated historical performance and projected changes in meteorological droughts using two drought indicators: the Standardized Precipitation Index (SPI; Mckee et al., 1993) and the Standardized Precipitation and Evapotranspiration Index (SPEI; Vicente-Serrano et al., 2010). SPEI was proposed by Vicente-Serrano, et al. (2010) as an improvement over SPI by incorporating variability of both precipitation and evapotranspiration for meteorological drought assessments.

SPI quantifies deviations in the accumulated precipitation from its historically 'normal' conditions. To calculate SPI, monthly precipitation values are first aggregated over *n*-months (accumulation period), a parametric statistical distribution is fitted, and the resulting quantiles are mapped onto a standard normal distribution. The final standardized value is the drought index, where positive and negative values correspond to wet and dry conditions, respectively. Several studies have utilized the Gamma distribution for SPI. For instance, Stagge et al. (2015) examined various probability distributions for fitting precipitation data with different accumulation scales across many grids over Europe and determined the Gamma distribution to be the most suitable. Additionally, other studies applied the Gamma distribution to 6-month accumulated precipitation for SPI across global grids (e.g., Asadi Zarch et al., 2017; Papalexiou et al., 2021; Spinoni et al., 2019, 2021).

SPEI also follows a similar statistical concept as SPI, except with aggregated monthly climatic water balance (precipitation minus potential evapotranspiration) instead of aggregated precipitation (Vicente-Serrano et al., 2010). For SPEI, the log-logistic distribution is utilized to fit the 6-month accumulated climatic water balance across all global grids, following Vicente-Serrano, et al. (2010) (e.g., Balting et al., 2021; Gu et al., 2020; Li et al., 2021; Spinoni et al., 2020).

Both SPI and SPEI can be computed over different timescales, reflecting the period over which data is accumulated before the drought index calculation. Smaller time scales (< 3 months) are applicable for soil moisture and agricultural droughts, and longer time scales (>12 months) for groundwater drought (WMO and GWP, 2016). A 6-month accumulation period is widely used as it filters out short-term anomalies while capturing the seasonal development of droughts (Balting et al., 2021; Naumann et al., 2018; Papalexiou et al., 2021; Touma et al., 2015). Hence, we aggregated precipitation and climatic water balance over 6 months to generate SPI-6 and SPEI-6 indices to capture droughts.

Both SPI and SPEI were calculated separately for observational products and each of the CMIP6 models (with two SSP scenarios per model from 1950 to 2100) to ensure that each model's drought metrics are calculated based on its own historical climatology. Distribution parameters for the fitted distributions in SPI and SPEI were estimated using the same dataset's historical data from 1950 to 2014. The wide 65-year period, beginning in 1950 ensures that major historical drought and pluvial events are included in the drought index development, thereby capturing historic variability more effectively (Chen et al., 2020; van der Schrier et al., 2013).

2.4. Drought event identification and characteristics

Positive and negative values of standardized drought indices, such as SPI and SPEI over a temporal scale, indicate wetter or drier conditions, respectively, compared to a historically "natural" mean. A drought event

is a period with consecutive index values below a specified threshold (Yevjevich, 1967). The lower the drought index value, the more severe the drought conditions. Drought index values can be used to categorize drought severity: mild ($0 \geq SPI > -1$), moderate ($-1 \geq SPI > -1.5$), severe ($-1.5 \geq SPI > -2$), and extreme ($-2 \geq SPI$) (McKee et al. 1993).

In this study, drought periods in the generated SPI and SPEI time-series for each grid in both the reference and CMIP6 dataset were identified by using a threshold (i.e., moderate to exceptional droughts). To filter out short-lived events that may recover quickly and to ensure that events detected are independent, criteria are defined for a drought's onset and termination, respectively. An onset is when the drought index falls and remains below −1 for a minimum of three consecutive months, and termination is when the index rises and remains above the threshold (−1) for a minimum of three consecutive months. Drought duration is the months between the initiation and termination of a drought, and drought severity is the integral of index values during a drought event. Drought frequency is the number of drought events detected in the analyzed period.

For both models and observations, drought characteristics, between 70°N and 70°S, were first evaluated in the native resolution and then re-gridded using bilinear interpolation (Wang et al., 2006) to a 1° resolution, to facilitate comparison as is common in multi-model analysis (e.g., Touma et al., 2015). We assess drought characteristics individually for each CMIP6 GCM and then combine them to create an unweighted multi-model mean drought response.

2.5. Historical analysis of CMIP6 drought performance

Evaluating model performance in a historical context is crucial to quantify uncertainties and identify systematic biases in drought simulations. We follow the approach of Ukkola et al. (2018), who provide a robust framework for evaluating the performance of CMIP models in simulating historical drought characteristics.

We first define a historical period from 1950 to 2014, during which sufficient observations of the variables necessary for drought analysis are available. For each land grid, we use these observations to create time series for both SPI and SPEI, which are then used to identify all drought events during the historical period. The average drought characteristics—such as duration, severity, and the total number of drought events—were calculated to create a grid-based dataset of observed drought characteristics.

We then applied the same procedure to each General Circulation Model (GCM), replacing observational data with the simulated output of the variables used in drought analysis. For each grid, GCM simulated outputs were used to develop SPI and SPEI time series from which we identified simulated drought events in the historical period. The average drought characteristics for each grid were then calculated and saved. This provides a gridded dataset of drought characteristics based on each GCM's simulation. Note GCM have different native resolution. We repeated this process for all GCMs. Since the resolutions of the GCMs and the reference dataset differ, we first re-grided all dataset's drought response to a common resolution. From here, we created a multi-model mean response by averaging the historical drought characteristics across the eight selected GCMs.

In Section 3.1, we discuss the bias of the multi-model mean drought characteristics from the reference dataset's drought characteristics in the historical period (1950–2014). Biases were calculated by simple differences between drought characteristics from GCMs and the observational/reference data. Using this approach, we identified global grids of poor model performance. A bias magnitude of more than 10 % from observations indicates inaccurate drought performance (Ukkola et al., 2018).

2.6. Projecting drought changes in future warming periods

We then utilized the models' future simulations to analyze projected changes in meteorological drought characteristics from a recent reference period to future 30-year periods when the projected global mean surface temperature is 1.5°, 2°, and 3 °C compared to the preindustrial period—a period just before significant human activities, particularly the burning of fossil fuels, began to alter Earth's climate. The preindustrial period is conventionally between 1850–1900, as defined in the IPCC Fifth and Sixth assessment reports (IPCC, 2014, 2021).

There are various approaches for assessing global and regional temperature changes (James et al., 2017); each has inherent constraints and uncertainties. We employed the commonly used and straightforward time sampling approach to estimate changes in Global Mean Surface Temperature (GMST) for selected GCM's. Similar to Wu et al. (2022), we selected the period from 1985 to 2014 as our reference time frame, with a GMST 0.66 °C higher than the preindustrial period. Whereas 1850–1900 serves as the preindustrial period, assessments of drought changes to future warmer periods often reference a recent baseline period (e.g., 1985–2014) that is more relevant to policymakers:

(i) The annual GMST time series is obtained by averaging the temperature of all grids over land and ocean. From this time series, the average GMST for the reference period from 1985 to 2014 is calculated and denoted as T_{ref}.
(ii) Since the GMST during the reference period is 0.66 °C higher than during preindustrial times, we estimate the preindustrial temperature by subtracting 0.66 °C from T_{ref}.
(iii) For any year in the historical and future periods, with the annual GMST denoted by T_{Future}, changes (anomalies) in GMST relative to the preindustrial period can be estimated in Eq. (2).

$$T_{change} = T_{Future} - (T_{ref} - 0.66) \quad (2)$$

(iv) To reduce annual variability in the GMST anomaly series (T_{change}), we apply a 30-year moving average. This moving average is centered around a "central year," spanning from 14 years before to 15 years after this year. The result is a smoothed time series where GMST anomalies are averaged over a 30-year period.
(v) From the resultant smoothed series, we identified the years when the 30-year smoothed GMST anomaly first crosses the required warming levels of 1.5 °C, 2 °C, and 3 °C.

While climate sensitivities may vary among models, shown as shaded regions in Fig. 1, we use the multi-model mean surface temperature, shown as bold lines in Fig. 1, to consistently identify future warming periods for SSP2-4.5 and SSP5-8.5 scenarios. The three global warming levels are reached later under SSP2-4.5 compared to SSP5-8.5, as expected, with only a few GCMs projecting a 3 °C warming under SSP2-4.5. Moreover, the drought characteristics at these warming levels show minimal differences between the two scenarios. The central year, representing the middle of the future 30-year period (15 years before and 14 years after), is identified from the multi-model mean GSMT anomaly when it first crosses the required warming levels of 1.5 °C, 2 °C, and 3 °C, as shown in Table 2. For SSP2-4.5, only models with GMST anomaly above 2 °C are used to derive the multi model-mean and the required crossing years (shown in brackets).

The projected changes in drought characteristics—duration, severity, and frequency—are derived from SPI and SPEI time series based on GCM outputs for different future warming periods. For each grid in a GCM, we compute the average historical drought characteristics during the reference period (1950–2014). The same process is then applied to future 30-year warming periods (1.5 °C, 2 °C, and 3 °C), using the GCM's output to derive future drought characteristics. Since GCMs operate at different spatial resolutions, we re-grid the drought responses to a common resolution, ensuring consistency across models. Finally, by averaging the drought responses from all eight CMIP6 models, we calculate the multi-model mean for both historical and future periods. The projected changes are determined by comparing the multi-model

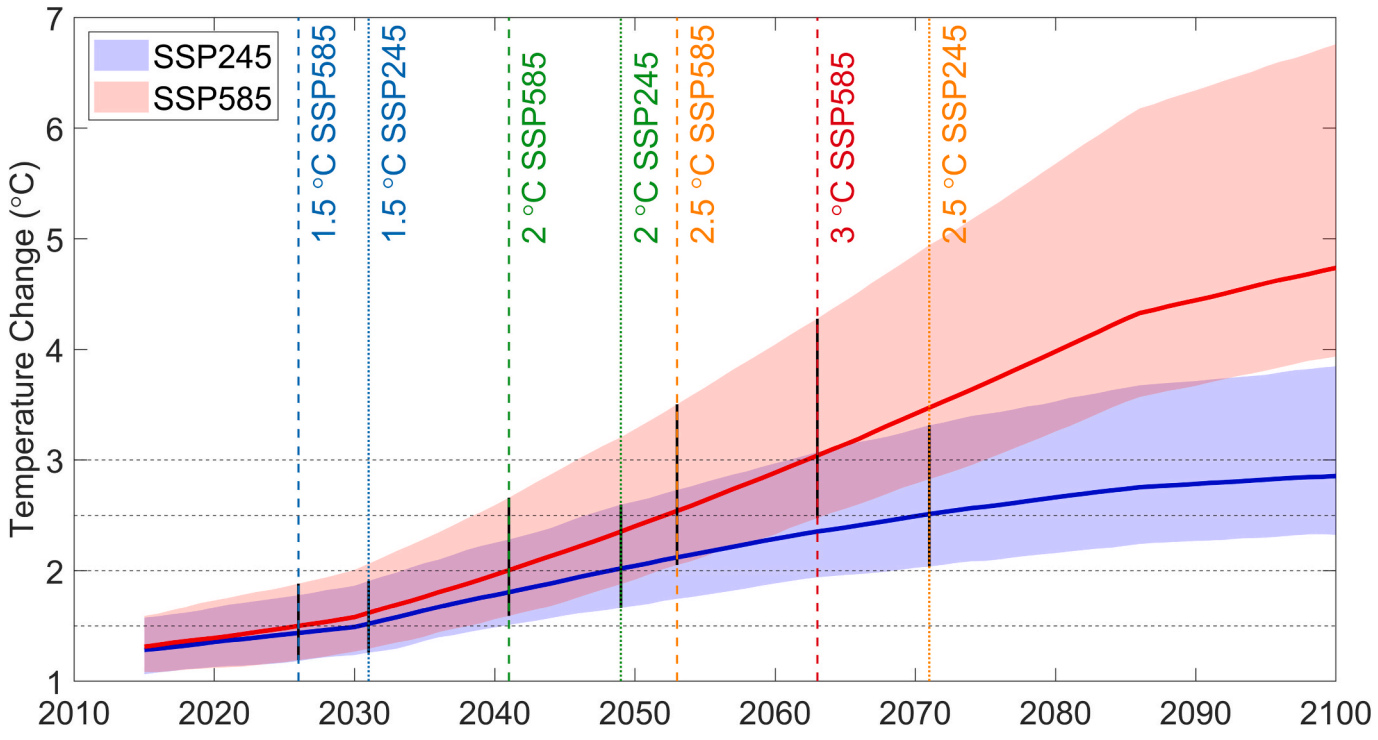

Fig. 1. Change in 30-year GMST from the prehistoric period 1850–1900. Dark lines show the multi-model mean change, while shaded regions show the range of GMST changes from CMIP6 GCMs.

Table 2
Central year corresponding to the 1.5, 2, 2.5, and 3 °C warming periods seen in multi-model mean surface temperature from selected models for different SSPs.

SSP	1.5 °C warming	2 °C warming	2.5 °C warming	3 °C warming
SSP245	2031 (2016–2045)	2049 (2034–2063)	(*2057*) (*2042–2071*)	(*2072*) (*2057–2086*)
SSP585	2026 (2011–2040)	2041 (2026–2055)	2053 (2038–2067)	2063 (2048–2077)

mean of the future periods against the historical period, which allows us to quantify how drought conditions (in terms of duration, severity, and frequency) are projected to change as global temperature rises.

3. Results and discussion

3.1. Multi-model and observed drought characteristics with Standardized precipitation index (SPI)

We compared the SPI and offline drought characteristics obtained from the multi-model mean against CRU observed data in the historical period and evaluate bias identifying areas where the multi-model means' drought characteristics differ from the observed dataset and the spread/range among CMIP6 models to identify inter-model variability of response in the historical period (Fig. 2).

The multi-model mean underestimates average historical duration and severity by more than 30 % in regions of Northeastern Canada, Northern South America, Central Africa, and Asia (Fig. 2g and 2i). Over the same regions, it overestimates the frequency of droughts by 20 to 30 % (Fig. 2h). Although the multi-model mean duration of SPI6 droughts is similar to the 5–6 month mean observed duration for most regions across the globe, it shows lesser spatial variations. For the average drought duration, the multi-model mean shows good performance (−10 % < bias < 10 %) over 46.3 %, overestimation (bias > +10 %) over 11 %, and underestimation (bias < -10 %) over 43.7 % of land grids (Fig. 2g). Whereas the multi-model mean shows much more spatial variations, it also performs well for drought frequency over 46.4 % of grids while overestimating and underestimating frequency in 45 % and 8.6 % of land grids, respectively (Fig. 2h). In terms of drought severity, the performance of the multi-model mean is similar to the performance shown for drought durations: 41.2 % good performance, 47.8 % underestimation, and 11 % overestimation of severity on land grids, compared to the observed dataset (Fig. 2i). Stippling across most regions indicates agreement among models for direction of bias in drought duration and severity (Fig. 2g and 2i) and a reduced variability for both metrics (Fig. 2j and 2 l). However, the absence of stippling for frequency (Fig. 2h) and the observed wider variability (Fig. 2k) suggest that models exhibit lower agreement regarding drought frequency than duration and severity.

Individual models display drought characteristics that align with observations in certain regions but can vary significantly in others (Fig. S1). This variation underscores the importance of multi-model evaluation. While individual models demonstrate good performance on less than 40 % of the land grids, the multi-model mean shows a slightly better performance, with a greater fraction of land showing good performance for drought duration, frequency, and severity (Fig. S1). Previous evaluations of SPI drought characteristics from CMIP5 and CMIP6 models against observed datasets also showed good model agreement for multiple drought metrics over at least 50 % of land fraction (Papalexiou et al., 2021; Ukkola et al., 2018, 2020). Regions such as the Amazon, Central Africa, and Asia exhibit a higher magnitude of multi-model bias and correspond to areas with historically higher drought duration and severity. This observation aligns with the findings of Papalexiou et al. (2021), where reduced agreement is seen in these regions, characterized by high observed drought statistics. This suggests that while CMIP6 models effectively capture average drought characteristics on a global scale, their accuracy declines significantly in replicating conditions of extreme drought severity and duration.

It is also important to note that the evaluated drought statistics may also be influenced by the methodologies. Ukkola et al. (2018) evaluated CMIP5 models for moderate, severe, and extreme SPI3 droughts

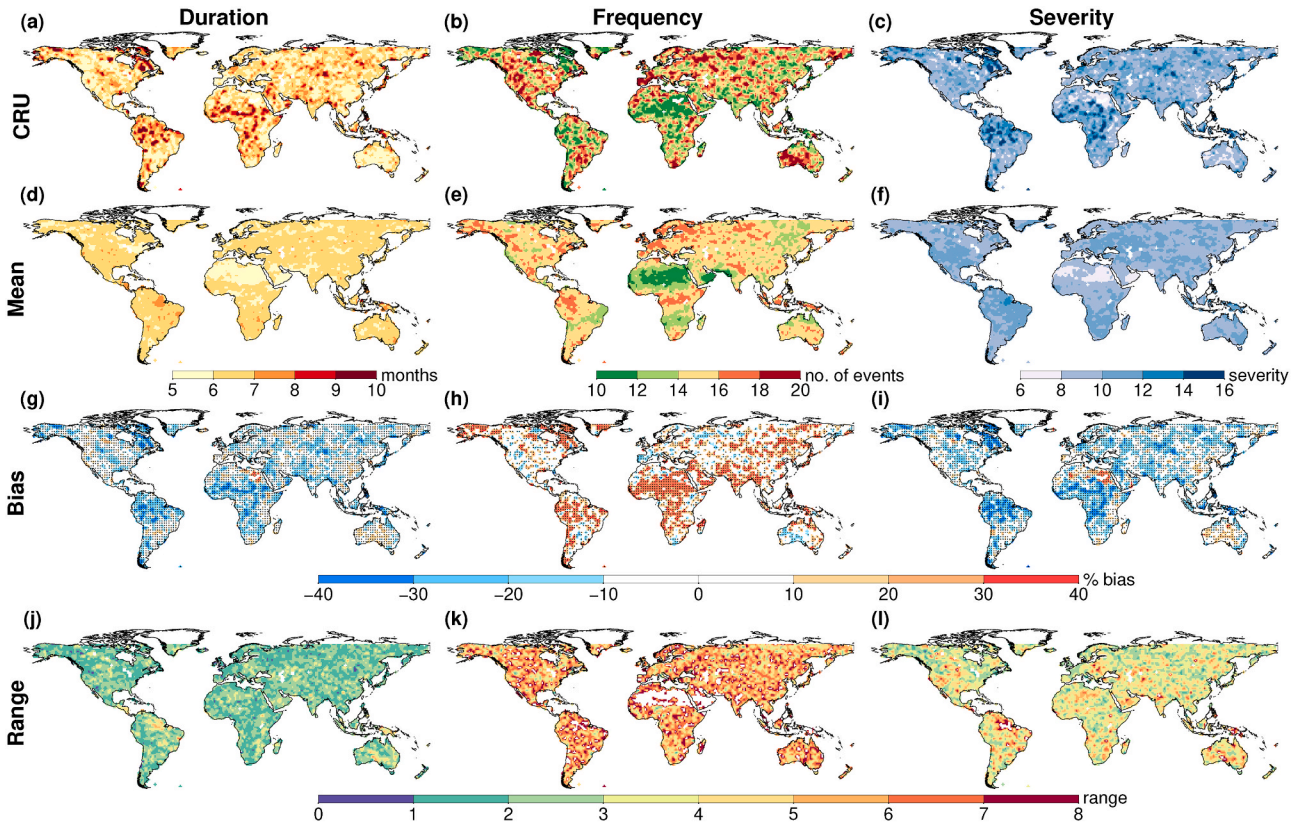

Fig. 2. Observed (a, b, and c) and CMIP6 multi-model mean (d, e, and f) drought characteristics for all droughts with SPI6 < -1 in the historical period 1950–2014. Bias (g, h, and i) shows the difference in average drought characteristics against observations. The intermodal range (j, k, and l) shows the difference between the 10th and 90th percentile of SPI drought characteristics from the selected models. Stippling in (g), (h), and (i) shows where more than 75 % of models (6 of 8) agree with the direction(sign) of multi-model mean bias.

individually while removing droughts of a duration larger than eight months. They report a lesser magnitude of bias for the average duration, with positive bias only in the northern African region, whereas regions showing positive bias for frequency, exceeding + 30 %, were similarly found in Central and Northern Africa and Amazon basin regions. Hence, CMIP6 models show lesser agreement and higher biases when multiple levels of severity and longer drought events are considered together in the analysis.

3.2. Multi-model and observed drought characteristics with Standardized Precipitation-Evapotranspiration index (SPEI)

Building on our previous analysis of precipitation-based drought characteristics, we further assessed CMIP6 models' performance in simulating droughts using SPEI. SPEI incorporates both precipitation and evapotranspiration, offering a more comprehensive view of drought conditions influenced by moisture supply and demand. We examined how well the multi-model mean captures SPEI-based offline drought characteristics in the historical period by evaluating the bias from the observed dataset's drought characteristics and the inter-model spread from the individual models (Fig. 3).

Contrary to SPI results, the CMIP6 models' SPEI-based assessments reveal greater spatial variability in drought duration and severity, more closely mirroring the observed dataset (Fig. 2d and 2f). Both SPI and SPEI analyses show that spatially, average drought duration aligns closely with average drought severity, exhibiting similar biases and performance levels for these characteristics. The pattern of duration and severity biases being inversely related to the bias in frequency is evident in both SPI and SPEI evaluations. Consequently, there are two predominant patterns of divergence observed in the average drought characteristics from the multi-model mean: either an overestimation of drought duration and severity with an underestimation of frequency or the reverse. This results in the multi-model mean either predicting average drought characteristics with shorter durations and lesser severity but higher frequency or longer and more severe droughts with lower frequency.

Regions where the multi-model mean overestimates duration and severity by more than 30 % and underestimates frequency by more than 20 % relative to observations include Eastern South America, Western and Southeastern Africa, Central Europe, Eastern Asia, and Australia. Conversely, regions showing an underestimation of duration and severity by more than 30 % and an overestimation of frequency by 20 % include smaller areas within the Amazon basin and larger areas in Northeastern and Central Africa, the Arabian Peninsula, and Central Asia. This tendency of the multi-model mean—presenting shorter durations, lesser severity, and greater frequency than observed—parallels multi-model mean's performance for SPI drought characteristics. The multi-model mean achieves a good agreement ($|bias| < 10\%$) over approximately 43 % of land grids. However, both positive and negative biases are observed over 30 % and 25 % of land grids, respectively, contrasting with the SPI results, which indicate about 40 % of land areas exhibited a negative bias against observed drought duration and severity and a positive bias for frequency. Stippling across most regions indicates a consensus among models regarding the direction of the multi-model mean bias (Fig. 3g, 3h, and 3i). The inter-model variability for duration and severity is lower at northern latitudes across North America, Europe, and Asia but higher in Northeastern South America, North Africa, and the Arabian Peninsula. For SPEI drought frequency, significant inter-model variability is noted in Northern South America, Africa, and the Arabian Peninsula.

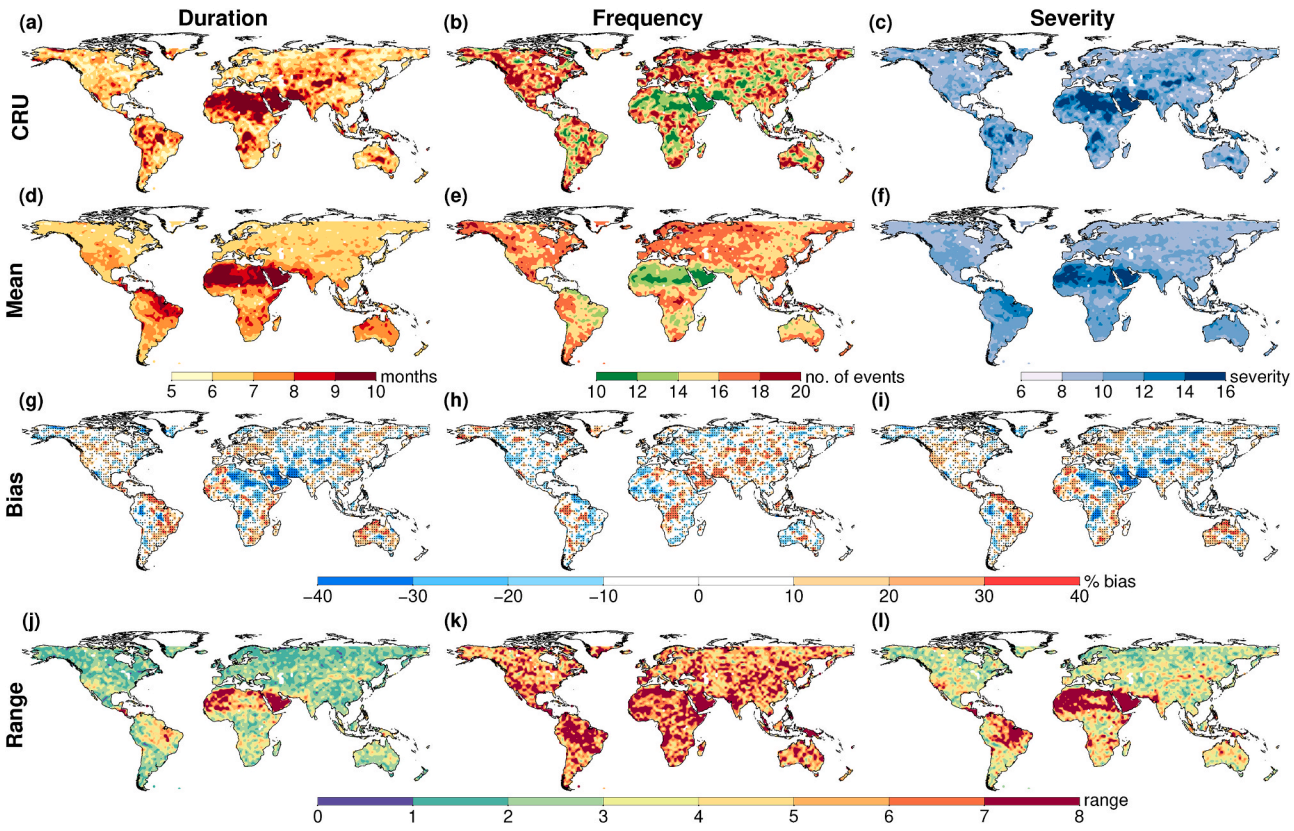

Fig. 3. Observed (a, b, and c) and CMIP6 multi-model mean (d, e, and f) drought characteristics for all droughts with SPEI-6 < -1 in the historical period 1950–2014 with multi-model mean bias (g, h, and i) and intermodal range (j, k, and l) from the selected models. Stippling in (g), (h), and (i) shows where more than 75 % of models (6 of 8) agree with the direction(sign) of multi-model mean bias.

Few studies have evaluated SPEI drought characteristics from CMIP6 models against observed datasets. Spinoni et al. (2020, 2021) assessed the bias in frequency and severity of droughts using an ensemble of high-resolution CMIP5 Regional Climate Models (RCM) against observations. They reported that the ensemble median for CMIP5 models exhibited low bias (less than 5 % in magnitude) for both frequency and severity of SPEI12 droughts over the 1981–2010 historical period, covering over 50 % of global land grids. Our analysis reveals a similar pattern with widespread agreement across most global grids but also identifies regions with significantly larger biases in both duration and severity. Notably, the regions where Spinoni et al. (2020, 2021) observed biases exceeding 10 % in magnitude for CMIP5 models' frequency and severity closely align with our findings.

Many differences in individual model drought characteristics from observations can be seen over various regions (Fig. S2). The multi-model approach again shows improved performance, with over 43 % of land grids showing good agreement compared to the individual model performance, where good agreement is seen only over < 39 % of land grids (Fig. S2). Regions of high bias were observed where drought characteristics show high values, as seen in previous studies (Papalexiou et al., 2021; Ridder et al., 2021). Whereas agreement of biases indicates they are systematic, we note that increasing more ensemble members or using high-resolution downscaled climate model outputs such as Regional Climate Models (RCMs) from the Coordinated Regional-climate Downscaling Experiment (CORDEX; Giorgi and Gutowski, 2015) would result in better performance of multi-model mean in reproducing observed meteorological drought characteristics. Future drought projections should be critically evaluated in regions where high biases are observed—climate model outputs used for drought evaluations may perform better with bias correction techniques (Adeyeri et al., 2023; Wu et al., 2022).

3.3. Projected changes in meteorological droughts

In the previous sections, we evaluated the performance of CMIP6 multi-model mean in reproducing observed SPI6 and SPEI6 drought characteristics over global land grids, hence identifying regions of high bias where drought projections are likely to be affected. In this section, we evaluate changes in meteorological droughts from a recent reference period (1985–2014) to future 30-year periods when the global mean surface temperature has risen by 1.5°, 2°, and 3 °C. We discuss the results from SSP5-8.5 simulations, as they provide more robust projections, particularly with a larger number of models reaching warming levels above 2 °C (Table S1). The SSP2-4.5 simulations show similar projected drought changes, with the primary difference being the timing at which the warming targets are reached. We present projected changes as absolute differences in drought characteristics between a future warming period and the reference period. Additionally, regions where more than 75 % (6 of 8) models agree on the direction (sign) of multi-model change, are highlighted by stippling (Fig. 4 and Fig. 5).

3.3.1. Projected changes in SPI droughts

Fig. 4 presents the drought duration, frequency, and severity changes for SPI6 droughts in future warming periods of 1.5 °C, 2 °C, and 3 °C. Several distinct regions—Central North America, Northern and Southern South America, the Mediterranean, Southern Africa, East Asia, and Australia—are projected to experience an increase in all three drought characteristics as global temperature continues to increase. Projections at 1.5 °C indicate drought durations in these regions could extend by 1 to 2 months, with Southern South America potentially experiencing increases of up to 5 months under the 3 °C scenario. The frequency of droughts in these regions follows a similar pattern, with an initial rise of 2 to 4 additional occurrences at a 1.5 °C increase and a sharper rise of 6

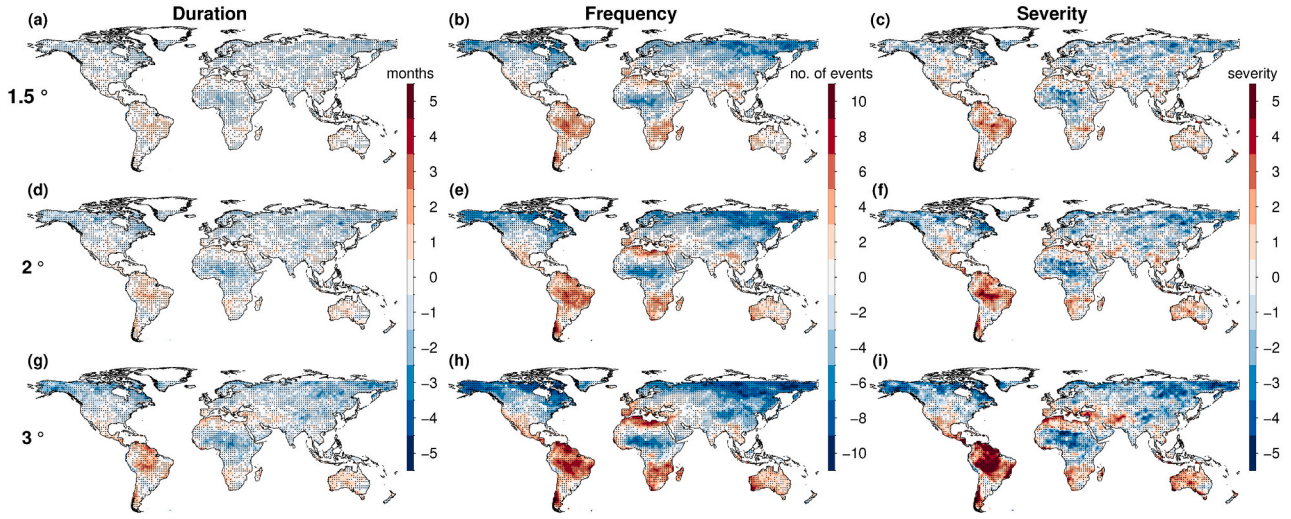

Fig. 4. Multi-model mean drought changes in future warming periods with SPI-6 and SSP5-8.5 simulations.

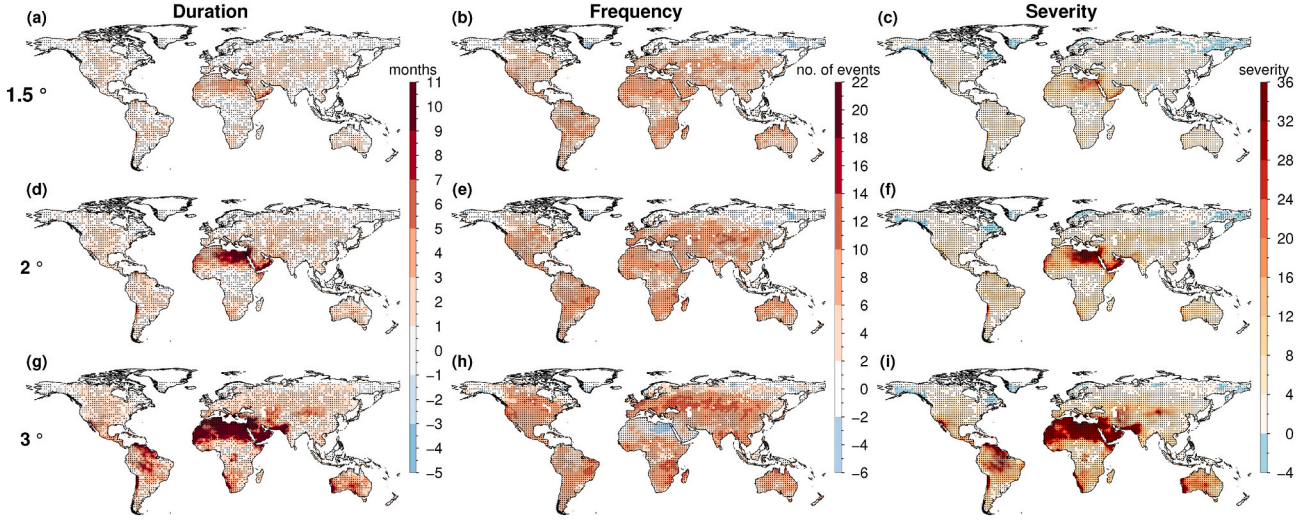

Fig. 5. Multi-model mean drought changes in future warming periods with SPEI-6 and SSP5-8.5 simulations.

to 8 events as warming progresses towards 3 °C. Drought severity, closely linked to duration and frequency, is also set to rise in these regions. At 1.5 °C warming, severity in these regions is projected to increase by scores ranging between 1.5 and 2.5, with Northern South America, Mediterranean region, and Australia seeing a dramatic increase of 3 to 4 points. This exacerbation of drought conditions is predicted to continue, with severity scores rising above 5 points in these regions as temperatures reach 2 °C and 3 °C.

A decrease in all three drought characteristics is projected across northern North America, Southeastern South America, Central Africa, Northern Europe, and most of Asia, with the decrease being more prominent as the warming progresses from 1.5 °C to 3 °C. While most of Australia is projected to experience increased drought duration, severity, and frequency, the Southeast region is projected to have reduced drought duration and severity. Notably, Southeast Asia and Central China diverge from this trend, showing increases in drought characteristics at 1.5 °C and 2 °C, which diminishes at 3 °C. While some models indicate the increased frequency in Southeast Asia, this is not uniformly agreed upon and may decrease at higher warming levels (Supplementary Information 2. Fig. S4).

3.3.2. *Projected changes in SPEI droughts*

Fig. 5 shows the projected drought characteristics, derived using SPEI6, at incremental global warming stages. In a 1.5 °C warmer world, most of the globe, except for the higher latitudes of North America, Europe, and Asia, is projected to experience longer droughts by at least 1 to 3 months. The largest increases in drought duration at 1.5 °C, are projected for Mediterranean Africa and the Arabian Peninsula, where drought duration increases by 7 to 9 months. These increases become even more widespread, with drought durations reaching 11 to 13 months at 2 °C and 3 °C of warming, compared to droughts in the recent reference period. Apart from Northern Africa and the Arabian Peninsula, several other regions, including Southern North America, Central America, Northern South America, Eastern and Southern Africa, the western regions of South Asia (including Pakistan and India), the Tibetan Plateau, and most of Australia, show significant increases in drought duration of up to 7 to 9 months when global warming reaches 2 °C. In a 3 °C warmer world, these increases become even more widespread, with drought durations reaching 11 to 13 months in the previously mentioned regions.

Drought frequency changes forecast a rise of 2 to 6 events across global land areas at a 1.5 °C warming level. The highest frequency increases in warmer worlds are seen across the mid-latitudes of both the

Northern and Southern Hemispheres. A rise of 8 to 10 events is projected for regions such as Western North America, the Canadian regions of North America, Eastern South America, most of Europe, and Central Asia in a 2 °C warmer period. By the 3 °C warmer period, the largest increases of 14 to 16 events, relative to the reference period, become evident and widespread in the mid-latitudes of North America, Europe, and Asia, along with parts of Southern South America, Southern Africa, and Southeast Asia.

At 1.5 °C warming, most global regions will face a modest increase in drought severity, while significant surges of 16 to 20 in severity scores are projected in Northern Africa and the Southern Arabian Peninsula. As warming increases to 2 °C, severity is also projected to increase for the Southwestern Coastal USA, Northern and Western Coastal Africa, and the Southern Arabian Peninsula. At 3 °C warming, projections highlight severe exacerbations in the Amazon Basin, North Africa, the Arabian Peninsula, Pakistan, Central Asia, and Australia, and where the western coast of the USA and southern Europe are also notably affected.

3.3.3. *Contrasting SPI and SPEI-based droughts: Role of temperature in meteorological drought assessments*

The projections of future drought characteristics under global warming at 1.5 °C, 2 °C, and 3 °C offer a detailed view of regional hydroclimate impacts. They demonstrate both agreement and disagreement when comparing assessments based on SPI and SPEI. We assess the fraction of land grids experiencing changes in drought conditions to examine how different indicators yield varying responses and highlight the regions exhibiting these differences. Drought characteristic changes are categorized as no change for absolute variations between −1 and + 1 compared to the reference—positive for changes above + 1, and negative for changes below −1.

Under a 1.5 °C scenario, using the SPI, a significant portion of land grids (85.3 %) showed no change in drought duration, whereas this was true for 56.1 % using the SPEI. Conversely, SPEI projections indicate that 43.1 % of the land grids are expected to experience positive changes (worsening conditions), a considerable increase from the 1.3 % projected by SPI. This trend becomes even more stark as the temperature rises to 2 °C and 3 °C, with positive changes in drought duration affecting 61.5 % and 74.9 % of land grids, respectively, according to SPEI, compared to 5.1 % and 12.9 % by SPI. The frequency of droughts follows a similar pattern, with SPI projecting that 22.1 % of land grids will experience an increase in drought frequency at 1.5 °C, while SPEI projections are much higher, at 80.3 %. This discrepancy widens further at 2 °C and 3 °C, with SPI indicating that 29.1 % and 33.4 % of land grids will experience more frequent droughts, while SPEI projects increase for 87.5 % and 86.5 %, respectively. Drought severity changes are also markedly different when comparing SPI and SPEI projections. While SPI suggests that 13.4 % of land grids will experience an increase in severity at 1.5 °C, SPEI suggests a much higher figure of 74.4 %. This disparity continues at higher warming levels, with 2 °C showing 19.6 % (SPI) versus 86.7 % (SPEI) and 3 °C showing 28.2 % (SPI) versus 91.8 % (SPEI) (Table 3).

Central North America, Northern South America, the Mediterranean, Southern Africa, East Asia, and Australia are all projected to see an increase in drought duration, frequency, and severity, under both SPI and SPEI at 1.5 °C, with these trends intensifying at 2 °C and 3 °C. Northern Africa and the Arabian Peninsula show significant drought severity and duration increases under both indices, especially as warming progresses.

However, where Northern North America, Southeastern South America, Europe, and most of Asia are anticipated to experience decreases in all drought characteristics, based on SPI, SPEI projects an increase in drought duration and severity for Central Asia and Western China, indicating a divergence in projections when temperature-based drought indicator is included. Northern Europe also exhibits a decrease in drought characteristics under SPI, whereas SPEI indicates an increase, especially in the frequency and severity of droughts in Eastern Europe and the Mediterranean. Conditions in Southeast Asia are somewhat ambiguous, with SPI suggesting possible increases or decreases in frequency, whereas SPEI projects initial moderate increases and significant increases at higher warming levels.

Table 3
The fraction of land grids shows negative and positive, and no changes, in drought characteristics in future warmer periods under SSP5-8.5. Fractions for SPEI projections are shown in brackets.

Warming	Negative change (%)	No Change (%)	Positive change (%)
Changes in drought duration			
1.5°	13.5 (0.8)	85.3 (56.1)	1.3 (43.1)
2°	27.7 (1.3)	67.2 (37.3)	5.1 (61.5)
3°	40.7 (1.6)	46.4 (23.5)	12.9 (74.9)
Changes in drought frequency			
1.5°	48 (5)	29.9 (14.7)	22.1 (80.3)
2°	52 (2.7)	18.9 (9.8)	29.1 (87.5)
3°	52 (7.4)	14.6 (6.1)	33.4 (86.5)
Changes in drought severity			
1.5°	25.9 (1.2)	60.7 (24.4)	13.4 (74.4)
2°	36.6 (1.2)	43.8 (12.1)	19.6 (86.7)
3°	43.6 (0.9)	28.1 (7.3)	28.2 (91.8)

Hydroclimate projections based solely on atmospheric precipitation deficit show that deficits pertaining to drought intensity is largest in the tropics, including the Amazon basin, and Mediterranean-type climate, including regions of the Mediterranean, Southwestern South America, Southern Africa, and Southwest Australia, whereas widespread drying will also be observed in Central America and Southern Australia (Cook et al., 2020; Ukkola et al., 2020). The results presented in this study for precipitation drought through SPI6 show similar regions projected to face increased drought duration and intensities in future periods. The changes in the average drought duration can also be seen in projected changes in Consecutive Dry Days (CDD) seen over many regions, such as stronger increases in the Mediterranean region and decreases in tropical Northern Africa (Almazroui et al., 2021). Similar to our results, the reversal of the increase in precipitation drought duration and severity at 1.5, 2 °C warming when reaching 3 °C over southern China was also observed by Wu et al. (2022) utilizing bias-corrected CMIP6 models at the local catchment scale.

Meteorological drought from an atmospheric deficit perspective- where the climatic water balance ($P-E$) accounts for the effects of local temperature changes to characterize droughts- shows much more significant increases in drought characteristics over most global regions than indicated by precipitation alone (Scheff & Frierson, 2015; Zhao & Dai, 2015). When temperature effects are incorporating, larger increases in drought characteristics become visible even in regions such as northern North America and Asia, where precipitation-based drought metrics show an alleviation of drought conditions provided precipitation increased in future warming periods (Wang et al., 2021). While evaluating ($P-E$) changes to the end of the century (2070–2099), Zhao and Dai, 2022 show that the $P-E$ flux changes are closely tied to changes in total runoff from CMIP models over most global land. They found that spatial patterns and magnitude of drying from $P-E$ flux changes are consistent across CMIP5 and CMIP6 model projections, showing widespread drying over North America, Europe, Western Asia, and Australia are tied to decreased precipitation, whereas increased runoff and projected alleviation of drought conditions are observed over Northeast and Southeast Asia regions are tied to increased precipitation in these regions. Whereas our projected changes to 1.5°, 2°, and 3 °C warming are realized sooner than the end of the century period in Zhao and Dai, 2022, for both SSP2-4.5 and SSP5-8.5 scenarios, similar areas of consistent drying in North America, the Mediterranean region, Southern Africa, and Australia were found in our projections as well. While $P-E$ flux changes suggest increased runoff, a decrease in surface and total soil moisture over Eastern Asia regions was found to be more closely tied to

projections of increased SPEI drought severity and frequency over the same regions in our study (Adeyeri et al., 2023; Tabari and Willems, 2022). Few studies project decreased frequency of meteorological droughts over the Indian subcontinent (Cook et al., 2020; Li et al., 2021). Aadhar and Mishra (2020) found significant increases in the frequency of both SPI12 and SPEI12 droughts in the Northwestern, Central and Eastern Indian Subcontinent, if the GCMs selected are able to better represent monsoon season precipitation. Wang et al. (2021) also found an increase in the probability of 6-month exceptional droughts by 5–10 % compared to the reference period in the latter half of the 21st century over the South Asia region. Our analysis shows an increase in SPEI6 drought frequency in Southern India at 1.5 °C warming, contrary to Aadhar and Mishra (2020), who report a decrease using SPEI12. The discrepancy likely stems from different PET estimation methods; the temperature-based method shows reduced drought frequency, while our FAO Penman-Monteith method indicates an increase for the same warming scenarios.

3.4. Projected changes in drought in different aridity zones

In the previous section, we evaluated the projected changes in average drought characteristics from eight CMIP6 models. These models presented a wide range of responses over global land areas, indicating that many regions may face increased or decreased drought risk due to changes in drought characteristics. In this section, we aggregate the projections for land grids based on their background aridity during the historical period. We analyze the aggregate changes and the variability over land grids of aridity classes for 1.5°, 2°, and 3 °C warming periods. Humid, transitional, and arid land areas were identified using the Aridity Index (AI), calculated as the ratio of annual PET to annual average precipitation, based on CRU TS4 observed data. The spatial distribution of land grids in the Humid ($AI \leq 0.9$), Transitional ($0.9 < AI \leq 2.25$), and Arid ($AI > 2.25$) aridity classes is depicted in Fig. 6 (Mukherjee & Mishra, 2021). Unlike the UNEP classification, which defines AI as the ratio of precipitation to potential evapotranspiration, our study inverts this ratio (PET to P). Consequently, the transitional class in our study, with AI values ranging from 0.9 to 2.25, includes regions at the edge of the humid and dry sub-humid classes as defined by UNEP (WAD, 2018).

The projected changes across humid and transitional regions (Fig. 6) show similar patterns emerging from both SPI and SPEI metrics. SPI anticipates a decrease in drought duration and severity for both regions, while an increase in frequency is expected as global warming progresses from 1.5° to 3 °C. On the contrary, SPEI projections indicate an increase in all three drought characteristics—duration, frequency, and severity. It is important to emphasize that such projections may not be uniformly distributed across all humid regions. For instance, according to SPI, the Amazon Basin is projected to experience increased droughts, contrasting with the reductions expected in humid parts of Northern Asia, Europe, and Equatorial Central Africa (Fig. 4).

In humid and transitional regions, increased evaporative demand and drier surfaces are expected to strengthen land–atmosphere interactions, especially under warming, leading to more frequent hot-dry events (Byrne, 2021). However, the role of natural vegetation in these interactions and its role under higher atmospheric CO_2 concentrations adds multiple uncertainties for future projections. The variability in water use efficiency in arid ecosystems is governed mainly by physical processes like evaporation, in contrast to semi-arid/sub-humid regions where biological processes like assimilation play a more significant role (Greve & Seneviratne, 2015). Amidst rising temperatures, Mediterranean Forests in transitional zones are experiencing escalated aridity, leading to increased forest browning and productivity declines (Miranda et al., 2023; Senf et al., 2020).

In contrast, arid regions present a divergent scenario. While SPI projections suggest no significant change in median drought duration, severity, or frequency across warming scenarios, SPEI projections highlight more pronounced changes. Under SPEI, the median drought duration is expected to increase by 2 to 3 months, the median frequency of drought events to rise by 3.5 to 4 events, and the median severity per event to escalate by 4.3 to 5.2 across the 1.5°, 2°, and 3 °C warming conditions. This suggests a trend towards more severe drought conditions in arid regions, as evidenced by the broader interquartile ranges seen in the SPEI analysis, indicative of greater variability and potential increases in drought attributes. SPEI, as computed by CMIP6 models, surpasses both PDSI and SPI in accurately capturing droughts in arid zones, displaying a consistently better performance, and thereby making it a preferable choice for predicting droughts when using CMIP6 data (Wu et al., 2024).

Recent increases in historical aridity are predominantly due to rising air temperatures, which suggest that precipitation increments cannot match the escalating evaporative demands driven by greenhouse gas-related warming (Ullah et al., 2022). Significantly, there is a need to differentiate between terrestrial aridity (A.I. index) and hydrological aridity (surface runoff). Studies have shown that increased aridity does not always correlate with decreased runoff, which is more sensitive to precipitation changes (Koutroulis, 2019). This implies that higher aridity could coexist with increased runoff, potentially leading to intensified land degradation and desertification (Huang et al., 2017; Panagos et al., 2022; Vicente-Serrano et al., 2020).

Dryland coverage could increase significantly by 2100, with substantial shifts in global land area towards drier types (Koutroulis, 2019; Lian et al., 2021). Arid regions are also projected to warm more than humid regions, presenting earlier threats such as decreased crop yields and increased droughts (Huang et al., 2017). Although CMIP6 models reasonably reproduce meteorological anomalies associated with droughts, they show limitations in accurately capturing mean drought characteristics in drylands.

4. Conclusions

We investigated the drought changes over global land projected by eight CMIP6 models under a moderate (SSP2-4.5) and a high (SSP5-8.5) emissions scenario. We first examined and compared the multi-model mean drought characteristics against observed drought characteristics in the historical period, using SPI and SPEI. Then, we use the climate model projections to show changes in mean drought characteristics in a future warming period. The main findings are summarized as follows:

1. CMIP6 models accurately capture average global drought characteristics via SPI and SPEI but they show significant biases in replicating extreme historical drought conditions in areas such as Northeastern Canada, Northern South America, Central Africa, and Asia.
2. The projected changes in SPI show a clear trend of increasing drought severity, frequency, and duration in southern hemisphere regions, including Southern South America, Southern Africa, and Australia, as global temperatures rise. In contrast, northern latitudes tend to experience a reduction in these drought characteristics as temperatures increase
3. For SPEI, the projected changes indicate a more pronounced and widespread increase in drought severity, frequency, and duration across both hemispheres as global temperatures rise. Regions such as Northern Africa, the Arabian Peninsula, the Amazon Basin, and parts of South Asia are expected to experience substantial drought intensification, especially at higher warming levels. Unlike SPI, the SPEI projections emphasize the significant role of temperature-driven evapotranspiration, leading to more severe drought conditions in many regions.
4. Drought projections across different aridity zones reveal that humid and transitional regions are expected to experience a decrease in drought duration and severity when using SPI, but SPEI forecasts an increase in all drought aspects under progressive global warming.

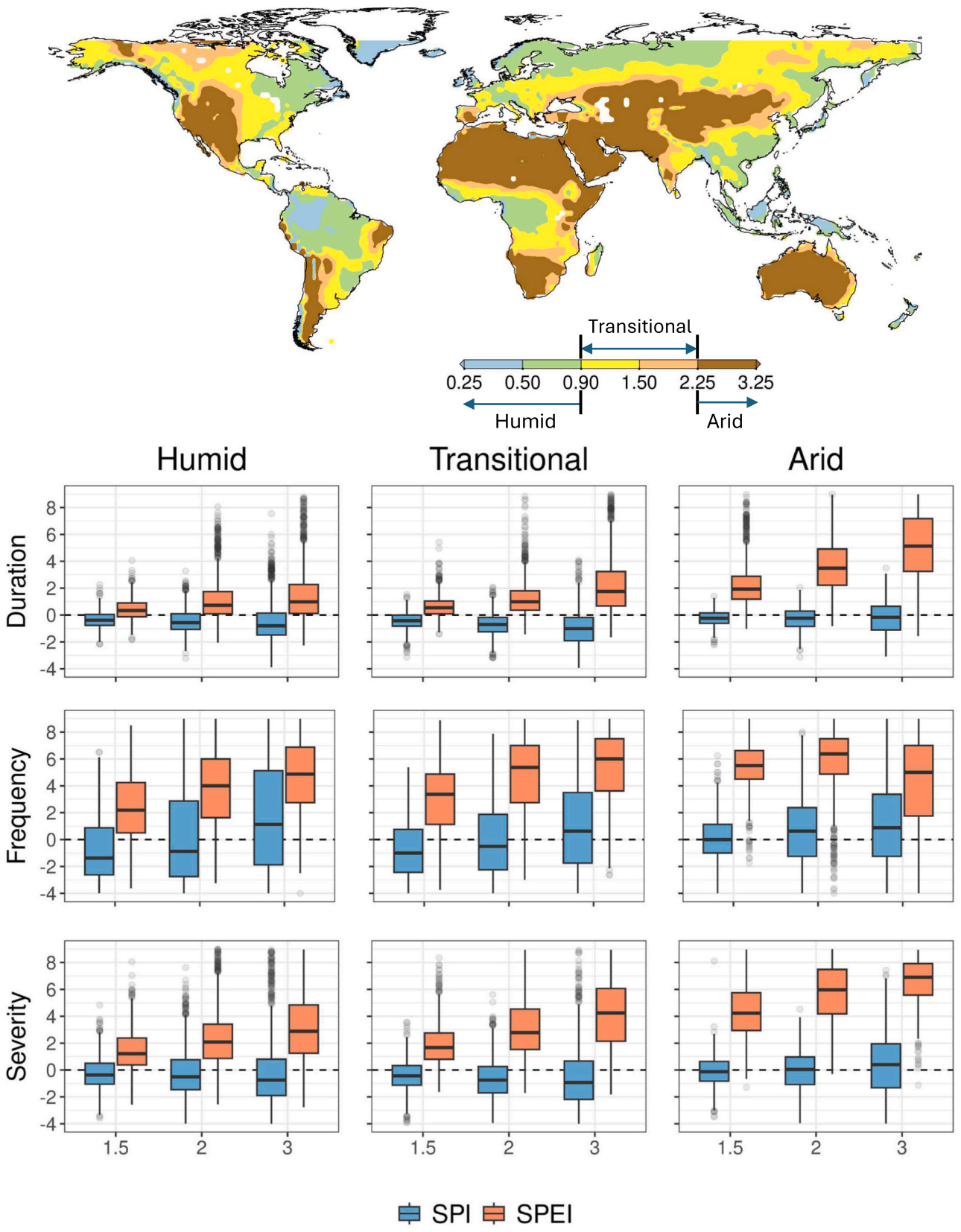

Fig. 6. Global aridity classification and projected changes in multi-model mean drought characteristics in different aridity regions based on SPI6 and SPEI6 at 1.5°, 2°, and 3 °C warmer periods under the SSP5-8.5 scenario. The bold horizontal line within each boxplot represents the median change, and the colored regions indicate the 25th and 75th percentile values of change over land grids in each aridity class. Vertical lines and dots denote changes lying within or outside the ± 1.5x interquartile range (IQR) range, where IQR is the difference between the 75th and 25th percentile of changes.

Arid regions display a stark contrast, with SPI suggesting little change but SPEI indicating significant increases in drought duration, frequency, and severity.

It is important to recognize the inherent uncertainties and limitations associated with our model simulations and the employment of Shared Socio-economic Pathways (SSPs), as shown in previous studies (Cook et al., 2018; Zhao and Dai, 2017). These limitations span various challenges, including the representation of physical processes like clouds formation and the inherent uncertainty in precipitation projections within GCMs (Knutti and Sedláček, 2013). The existing land surface models also exhibit shortcomings in adequately simulating complex hydrological subsurface processes, significantly contributing to the uncertainties characterizing drought projections (Berg et al., 2017). Furthermore, dynamical phenomena like atmospheric blocking, crucial for understanding climate extremes, are often inadequately represented by climate models and may be affected by biases (Davini & D'Andrea, 2020). The estimation of PET also introduces considerable uncertainty, which leads to biases in drought projections (Mukherjee et al., 2018). These limitations encompass the complex role of vegetation processes in a warming climate and varying climate sensitivities among different GCMs (Lemordant et al., 2018; Seneviratne & Hauser, 2020).

CRediT authorship contribution statement

Kunal Bhardwaj: Writing – original draft, Investigation, Formal analysis, Data curation. **Ashok Mishra:** Writing – review & editing, Supervision, Methodology, Funding acquisition, Conceptualization. **C. Prakash Khedun:** Writing – review & editing, Supervision, Methodology, Formal analysis.

Declaration of competing interest

The authors declare that they have no known competing financial interests or personal relationships that could have appeared to influence the work reported in this paper.

Acknowledgment

This study was supported by the National Science Foundation (NSF) award # 2422542. The computation of SPI was performed using the SCI package in R developed by Gudmundsson and Stagge (2015) https://cran.r-project.org/web/packages/SCI/index.html. For SPEI, we use the 'SPEI' package in R developed by Beguería and Vicente-Serrano (2017) https://cran.r-project.org/web/packages/SPEI/index.html.

Appendix A. Supplementary data

Supplementary data to this article can be found online at https://doi.org/10.1016/j.jhydrol.2025.133309.

Data availability

Data will be made available on request.

References

Aadhar, S., Mishra, V., 2020. Increased Drought Risk in South Asia under Warming Climate: Implications of Uncertainty in Potential Evapotranspiration Estimates. J. Hydrometeorol. 21 (12), 2979–2996. https://doi.org/10.1175/JHM-D-19-0224.1.

Adeyeri, O.E., Zhou, W., Laux, P., Ndehedehe, C.E., Wang, X., Usman, M., Akinsanola, A. A., 2023. Multivariate Drought Monitoring, Propagation, and Projection Using Bias-Corrected General Circulation Models. Earth's. Future 11 (4). https://doi.org/10.1029/2022EF003303.

AghaKouchak, A., Mirchi, A., Madani, K., Di Baldassarre, G., Nazemi, A., Alborzi, A., Anjileli, H., Azarderakhsh, M., Chiang, F., Hassanzadeh, E., Huning, L.S., Mallakpour, I., Martinez, A., Mazdiyasni, O., Moftakhari, H., Norouzi, H., Sadegh, M., Sadeqi, D., Van Loon, A.F., Wanders, N., 2021. Anthropogenic Drought: Definition, Challenges, and Opportunities. Rev. Geophys. 59 (2). https://doi.org/10.1029/2019RG000683.

Allen, R.G., Pereira, L.S., Raes, D., Smith, M., 1998. FAO Irrigation and drainage paper No. 56. Rome: Food and Agriculture Organization of the United Nations 56, e156.

Almazroui, M., Saeed, F., Saeed, S., Ismail, M., Ehsan, M.A., Islam, M.N., Abid, M.A., O'Brien, E., Kamil, S., Rashid, I.U., Nadeem, I., 2021. Projected Changes in Climate Extremes Using CMIP6 Simulations Over SREX Regions. Earth Syst. Environ. 5 (3), 481–497. https://doi.org/10.1007/s41748-021-00250-5.

Al-Yaari, A., Zhao, Y., Cheruy, F., & Thiery, W. (2023). Heatwave Characteristics in the Recent Climate and at Different Global Warming Levels: A Multimodel Analysis at the Global Scale. Earth's Future, 11(9). doi: 10.1029/2022EF003301.

Asadi Zarch, M.A., Sivakumar, B., Malekinezhad, H., Sharma, A., 2017. Future aridity under conditions of global climate change. J Hydrol (Amst) 554, 451–469. https://doi.org/10.1016/j.jhydrol.2017.08.043.

Balting, D.F., AghaKouchak, A., Lohmann, G., Ionita, M., 2021. Northern Hemisphere drought risk in a warming climate. Npj Clim. Atmos. Sci. 4 (1). https://doi.org/10.1038/s41612-021-00218-2.

Berg, A., Sheffield, J., Milly, P.C.D., 2017. Divergent surface and total soil moisture projections under global warming. Geophys. Res. Lett. 44 (1), 236–244. https://doi.org/10.1002/2016GL071921.

Bi, D., Dix, M., Marsland, S., O'Farrell, S., Sullivan, A., Bodman, R., Law, R., Harman, I., Srbinovsky, J., Rashid, H.A., Dobrohotoff, P., Mackallah, C., Yan, H., Hirst, A., Savita, A., Dias, F.B., Woodhouse, M., Fiedler, R., Heerdegen, A., 2020. Configuration and spin-up of ACCESS-CM2, the new generation Australian Community Climate and Earth System Simulator Coupled Model. Journal of Southern Hemisphere Earth Systems Science 70 (1), 225–251. https://doi.org/10.1071/ES19040.

Bjarke, N.R., Livneh, B., Barsugli, J.J., Pendergrass, A.G., Small, E.E., 2024. Evaluating Large-Storm Dominance in High-Resolution GCMs and Observations Across the Western Contiguous United States. Earth's. Future 12 (6). https://doi.org/10.1029/2023EF004289.

Burke, E.J., Brown, S.J., 2008. Evaluating uncertainties in the projection of future drought. J. Hydrometeorol. 9 (2), 292–299. https://doi.org/10.1175/2007JHM929.1.

Byrne, M.P., 2021. Amplified warming of extreme temperatures over tropical land. Nat. Geosci. 14 (11), 837–841. https://doi.org/10.1038/s41561-021-00828-8.

Chen, J., Brissette, F.P., Caya, D., 2020. Remaining error sources in bias-corrected climate model outputs. Clim. Change 162 (2), 563–582. https://doi.org/10.1007/s10584-020-02744-z.

Chen, J., Brissette, F.P., Chaumont, D., Braun, M., 2013. Finding appropriate bias correction methods in downscaling precipitation for hydrologic impact studies over North America. Water Resour. Res. 49 (7), 4187–4205. https://doi.org/10.1002/wrcr.20331.

Chiang, F., Mazdiyasni, O., AghaKouchak, A., 2021. Evidence of anthropogenic impacts on global drought frequency, duration, and intensity. Nat. Commun. 12 (1). https://doi.org/10.1038/s41467-021-22314-w.

Christian, J.I., Martin, E.R., Basara, J.B., Furtado, J.C., Otkin, J.A., Lowman, L.E.L., Hunt, E.D., Mishra, V., Xiao, X., 2023. Global projections of flash drought show increased risk in a warming climate. Commun. Earth Environ. 4 (1). https://doi.org/10.1038/s43247-023-00826-1.

Cook, B.I., Mankin, J.S., Anchukaitis, K.J., 2018. Climate Change and Drought: From Past to Future. Curr Clim Change Rep. https://doi.org/10.1007/s40641-018-0093-2.

Cook, B.I., Mankin, J.S., Marvel, K., Williams, A.P., Smerdon, J.E., Anchukaitis, K.J., 2020. Twenty-First Century Drought Projections in the CMIP6 Forcing Scenarios. Earth's. Future 8 (6). https://doi.org/10.1029/2019EF001461.

Dai, A., Zhao, T., 2017. Uncertainties in historical changes and future projections of drought. Part I: estimates of historical drought changes. Clim. Change 144 (3), 519–533. https://doi.org/10.1007/s10584-016-1705-2.

Davini, P., D'Andrea, F., 2020. From CMIP3 to CMIP6: Northern Hemisphere Atmospheric Blocking Simulation in Present and Future Climate. J. Clim. 33 (23), 10021–10038. https://doi.org/10.1175/JCLI-D-19-0862.1.

Diffenbaugh, N.S., Swain, D.L., Touma, D., Lubchenco, J., 2015. Anthropogenic warming has increased drought risk in California. PNAS 112 (13), 3931–3936. https://doi.org/10.1073/pnas.1422385112.

Dunne, J.P., Horowitz, L.W., Adcroft, A.J., Ginoux, P., Held, I.M., John, J.G., Krasting, J. P., Malyshev, S., Naik, V., Paulot, F., Shevliakova, E., Stock, C.A., Zadeh, N., Balaji, V., Blanton, C., Dunne, K.A., Dupuis, C., Durachta, J., Dussin, R., Zhao, M., 2020. The GFDL Earth System Model Version 4.1 (GFDL-ESM 4.1): Overall Coupled Model Description and Simulation Characteristics. J. Adv. Model. Earth Syst. 12 (11), e2019MS002015. https://doi.org/10.1029/2019MS002015.

Eyring, V., Bony, S., Meehl, G.A., Senior, C.A., Stevens, B., Stouffer, R.J., Taylor, K.E., 2016. Overview of the Coupled Model Intercomparison Project Phase 6 (CMIP6) experimental design and organization. Geosci. Model Dev. 9 (5), 1937–1958. https://doi.org/10.5194/gmd-9-1937-2016.

Giorgi, F., & Gutowski, W. J. (2015). Regional Dynamical Downscaling and the CORDEX Initiative. In Annual Review of Environment and Resources (Vol. 40, pp. 467–490). Annual Reviews Inc. doi: 10.1146/annurev-environ-102014-021217.

Gimeno-Sotelo, L., Sorí, R., Nieto, R., Vicente-Serrano, S.M., Gimeno, L., 2024. Unravelling the origin of the atmospheric moisture deficit that leads to droughts. Nature Water. https://doi.org/10.1038/s44221-023-00192-4.

Greve, P., Seneviratne, S.I., 2015. Assessment of future changes in water availability and aridity. Geophys. Res. Lett. 42 (13), 5493–5499. https://doi.org/10.1002/2015GL064127.

Gu, L., Chen, J., Yin, J., Sullivan, S.C., Wang, H.-M., Guo, S., Zhang, L., Kim, J.-S., 2020. Projected increases in magnitude and socioeconomic exposure of global droughts in

1.5 and 2 °C warmer climates. Hydrol. Earth Syst. Sci. 24 (1), 451–472. https://doi.org/10.5194/hess-24-451-2020.
Gusain, A., Ghosh, S., Karmakar, S., 2020. Added value of CMIP6 over CMIP5 models in simulating Indian summer monsoon rainfall. Atmos Res 232. https://doi.org/10.1016/j.atmosres.2019.104680.
Huang, J., Li, Y., Fu, C., Chen, F., Fu, Q., Dai, A., Shinoda, M., Ma, Z., Guo, W., Li, Z., Zhang, L., Liu, Y., Yu, H., He, Y., Xie, Y., Guan, X., Ji, M., Lin, L., Wang, S., Wang, G., 2017. Dryland climate change: Recent progress and challenges. Rev. Geophys. 55 (3), 719–778. https://doi.org/10.1002/2016RG000550.
IPCC, 2021: *Climate Change 2021: The Physical Science Basis. Contribution of Working Group I to the Sixth Assessment Report of the Intergovernmental Panel on Climate Change* [Masson-Delmotte, V., P. Zhai, A. Pirani, S.L. Connors, C. Péan, S. Berger, N. Caud, Y. Chen, L. Goldfarb, M.I. Gomis, M. Huang, K. Leitzell, E. Lonnoy, J.B.R. Matthews, T. K. Maycock, T. Waterfield, O. Yelekçi, R. Yu, and B. Zhou (eds.)]. Cambridge University Press, Cambridge, United Kingdom and New York, NY, USA, In press, doi: http://10.1017/9781009157896.
James, R., Washington, R., Schleussner, C.F., Rogelj, J., Conway, D., 2017. Characterizing half-a-degree difference: a review of methods for identifying regional climate responses to global warming targets. In. Wiley Interdisciplinary Reviews: Climate Change Vol. 8, Issue 2, Wiley-Blackwell. https://doi.org/10.1002/wcc.457.
Khedun, C.P., Singh, V.P., 2014. Climate Change, Water, and Health: A Review of Regional Challenges. Water Qual Expo Health 6 (1–2), 7–17. https://doi.org/10.1007/s12403-013-0107-1.
Koutroulis, A.G., 2019. Dryland changes under different levels of global warming. Sci. Total Environ. 655, 482–511. https://doi.org/10.1016/j.scitotenv.2018.11.215.
Lehner, F., Coats, S., Stocker, T.F., Pendergrass, A.G., Sanderson, B.M., Raible, C.C., Smerdon, J.E., 2017. Projected drought risk in 1.5°C and 2°C warmer climates. Geophys Res Lett 44, 7419–7428. https://doi.org/10.1002/2017GL074117.
Lemordant, L., Gentine, P., Swann, A.S., Cook, B.I., Scheff, J., 2018. Critical impact of vegetation physiology on the continental hydrologic cycle in response to increasing CO2. PNAS 115 (16), 4093–4098. https://doi.org/10.1073/pnas.1720712115.
Lenton, T.M., Ciscar, J.C., 2013. Integrating tipping points into climate impact assessments. Clim Change 117, 585–597. https://doi.org/10.1007/s10584-012-0572-8.
Li, H., Li, Z., Chen, Y., Xiang, Y., Liu, Y., Kayumba, P.M., Li, X., 2021. Drylands face potential threat of robust drought in the CMIP6 SSPs scenarios. Environ. Res. Lett. 16 (11). https://doi.org/10.1088/1748-9326/ac2bce.
Lian, X., Piao, S., Chen, A., Huntingford, C., Fu, B., Li, L. Z. X., Huang, J., Sheffield, J., Berg, A. M., Keenan, T. F., McVicar, T. R., Wada, Y., Wang, X., Wang, T., Yang, Y., & Roderick, M. L. (2021). Multifaceted characteristics of dryland aridity changes in a warming world. In Nature Reviews Earth and Environment (Vol. 2, Issue 4, pp. 232–250). Springer Nature. doi: 10.1038/s43017-021-00144-0.
Liu, W., Sun, F., Lim, W.H., Zhang, J., Wang, H., Shiogama, H., Zhang, Y., 2018. Global drought and severe drought-affected populations in 1.5 and 2 °C warmer worlds. Earth Syst. Dyn. 9 (1), 267–283. https://doi.org/10.5194/esd-9-267-2018.
Maraun, D. (2016). Bias Correcting Climate Change Simulations - a Critical Review. In Current Climate Change Reports (Vol. 2, Issue 4, pp. 211–220). Springer. doi: 10.1007/s40641-016-0050-x.
Mauritsen, T., Bader, J., Becker, T., Behrens, J., Bittner, M., Brokopf, R., Brovkin, V., Claussen, M., Crueger, T., Esch, M., Fast, I., Fiedler, S., Fläschner, D., Gayler, V., Giorgetta, M., Goll, D.S., Haak, H., Hagemann, S., Hedemann, C., Roeckner, E., 2019. Developments in the MPI-M Earth System Model version 1.2 (MPI-ESM1.2) and Its Response to Increasing CO 2. J. Adv. Model. Earth Syst. 11 (4), 998–1038. https://doi.org/10.1029/2018MS001400.
Mckee, T.B., Doesken, N.J., Kleist, J., 1993. The relationship of drought frequency and duration to time scales. In Eighth Conference on Applied Climatology.
Michalek, A.T., Villarini, G., Kim, T., 2024. Understanding the Impact of Precipitation Bias-Correction and Statistical Downscaling Methods on Projected Changes in Flood Extremes. Earth's. Future 12 (3). https://doi.org/10.1029/2023EF004179.
Milly, P.C.D., Dunne, K.A., 2016. Potential evapotranspiration and continental drying. Nat Clim Chang 6, 946–949. https://doi.org/10.1038/nclimate3046.
Miranda, A., Syphard, A.D., Berdugo, M., Carrasco, J., Gómez-González, S., Ovalle, J.F., Delpiano, C.A., Vargas, S., Squeo, F.A., Miranda, M.D., Dobbs, C., Mentler, R., Lara, A., Garreaud, R., 2023. Widespread synchronous decline of Mediterranean-type forest driven by accelerated aridity. Nat. Plants 9 (11), 1810–1817. https://doi.org/10.1038/s41477-023-01541-7.
Mishra, A.K., Singh, V.P., 2010. A review of drought concepts. Journal of Hydrology 391 (1–2), 202–216. https://doi.org/10.1016/j.jhydrol.2010.07.012.
Mishra, V., Aadhar, S., Mahto, S.S., 2021. Anthropogenic warming and intraseasonal summer monsoon variability amplify the risk of future flash droughts in India. Npj Clim. Atmos. Sci. 4 (1). https://doi.org/10.1038/s41612-020-00158-3.
Mukherjee, S., Mishra, A.K., 2021. Increase in Compound Drought and Heatwaves in a Warming World. Geophys. Res. Lett. 48 (1). https://doi.org/10.1029/2020GL090617.
Mukherjee, S., Mishra, A., Trenberth, K.E., 2018. Climate change and drought: a perspective on drought indices. Current Climate Change Reports 4 (2), 145–163.
Müller, W.A., Jungclaus, J.H., Mauritsen, T., Baehr, J., Bittner, M., Budich, R., Bunzel, F., Esch, M., Ghosh, R., Haak, H., Ilyina, T., Kleine, T., Kornblueh, L., Li, H., Modali, K., Notz, D., Pohlmann, H., Roeckner, E., Stemmler, I., Marotzke, J., 2018. A Higher-resolution Version of the Max Planck Institute Earth System Model (MPI-ESM1.2-HR). Journal of Advances in Modeling Earth Systems 10 (7), 1383–1413. https://doi.org/10.1029/2017MS001217.
Nasrollahi, N., AghaKouchak, A., Cheng, L., Damberg, L., Phillips, T.J., Miao, C., Hsu, K., Sorooshian, S., 2015. How well do CMIP5 climate simulations replicate historical trends and patterns of meteorological droughts? Water Resour. Res. 51 (4), 2847–2864. https://doi.org/10.1002/2014WR016318.
Naumann, G., Alfieri, L., Wyser, K., Mentaschi, L., Betts, R.A., Carrao, H., Spinoni, J., Vogt, J., Feyen, L., 2018. Global Changes in Drought Conditions Under Different Levels of Warming. Geophys Res Lett 45, 3285–3296. https://doi.org/10.1002/2017GL076521.
Naumann, G., Cammalleri, C., Mentaschi, L., Feyen, L., 2021. Increased economic drought impacts in Europe with anthropogenic warming. Nat. Clim. Chang. 11 (6), 485–491. https://doi.org/10.1038/s41558-021-01044-3.
Norris, J., Chen, D., Hall, A., Thackeray, C.W., 2022. Moisture-Budget Drivers of Global Projections of Meteorological Drought From Multiple GCM Large Ensembles. J. Geophys. Res. Atmos. 127 (24). https://doi.org/10.1029/2022JD037745.
Otto, F. E. L., Wolski, P., Lehner, F., Tebaldi, C., Van Oldenborgh, G. J., Hogesteeger, S., Singh, R., Holden, P., Fučkar, N. S., Odoulami, R. C., & New, M. (2018). Anthropogenic influence on the drivers of the Western Cape drought 2015-2017. Environmental Research Letters, 13(12). doi: 10.1088/1748-9326/aae9f9.
Panagos, P., Borrelli, P., Matthews, F., Liakos, L., Bezak, N., Diodato, N., Ballabio, C., 2022. Global rainfall erosivity projections for 2050 and 2070. J. Hydrol. 610. https://doi.org/10.1016/j.jhydrol.2022.127865.
Papalexiou, S.M., Rajulapati, C.R., Andreadis, K.M., Foufoula-Georgiou, E., Clark, M.P., Trenberth, K.E., 2021. Probabilistic Evaluation of Drought in CMIP6 Simulations. Earth's. Future 9 (10). https://doi.org/10.1029/2021EF002150.
Peña-Angulo, D., Vicente-Serrano, S.M., Domínguez-Castro, F., Murphy, C., Reig, F., Tramblay, Y., Trigo, R.M., Luna, M.Y., Turco, M., Noguera, I., Aznárez-Balta, M., García-Herrera, R., Tomas-Burguera, M., El Kenawy, A., 2020. Long-term precipitation in Southwestern Europe reveals no clear trend attributable to anthropogenic forcing. Environmental Research Letters 15. https://doi.org/10.1088/1748-9326/ab9c4f.
Richardson, D., Black, A.S., Irving, D., Matear, R.J., Monselesan, D.P., Risbey, J.S., Squire, D.T., Tozer, C.R., 2022. Global increase in wildfire potential from compound fire weather and drought. Npj Clim. Atmos. Sci. 5 (1). https://doi.org/10.1038/s41612-022-00248-4.
Ridder, N. N., Pitman, A. J., & Ukkola, A. M. (2021). Do CMIP6 Climate Models Simulate Global or Regional Compound Events Skillfully? In Geophysical Research Letters (Vol. 48, Issue 2). Blackwell Publishing Ltd. doi: 10.1029/2020GL091152.
Ritchie, P.D.L., Clarke, J.J., Cox, P.M., Huntingford, C., 2021. Overshooting tipping point thresholds in a changing climate. Nature. https://doi.org/10.1038/s41586-021-03263-2.
Rivera, J.A., Arnould, G., 2020. Evaluation of the ability of CMIP6 models to simulate precipitation over Southwestern South America: Climatic features and long-term trends (1901–2014). Atmos Res 241. https://doi.org/10.1016/j.atmosres.2020.104953.
Scheff, J., Frierson, D.M.W., 2015. Terrestrial aridity and its response to greenhouse warming across CMIP5 climate models. J. Clim. 28 (14), 5583–5600. https://doi.org/10.1175/JCLI-D-14-00480.1.
Seneviratne, S.I., Hauser, M., 2020. Regional Climate Sensitivity of Climate Extremes in CMIP6 Versus CMIP5 Multimodel Ensembles. Earth's. Future 8 (9). https://doi.org/10.1029/2019EF001474.
Senf, C., Buras, A., Zang, C.S., Rammig, A., Seidl, R., 2020. Excess forest mortality is consistently linked to drought across Europe. Nat. Commun. 11 (1). https://doi.org/10.1038/s41467-020-19924-1.
Singh, V.P., Khedun, C.P., Mishra, A.K., 2014. Water, Environment, Energy, and Population Growth: Implications for Water Sustainability under Climate Change. J. Hydrol. Eng. 19 (4), 667–673. https://doi.org/10.1061/(ASCE)HE.1943-5584.0000866.
Smith, A., 2020. 2010–2019: a landmark decade of US billion-dollar weather and climate disasters. National Oceanic and Atmospheric. Administration.
Spinoni, J., Barbosa, P., Bucchignani, E., Cassano, J., Cavazos, T., Cescatti, A., Christensen, J.H., Christensen, O.B., Coppola, E., Evans, J.P., Forzieri, G., Geyer, B., Giorgi, F., Jacob, D., Katzfey, J., Koenigk, T., Laprise, R., Lennard, C.J., Kurnaz, M.L., Dosio, A., 2021. Global exposure of population and land-use to meteorological droughts under different warming levels and SSPs: A CORDEX -based study. Int. J. Climatol. 41 (15), 6825–6853. https://doi.org/10.1002/joc.7302.
Spinoni, J., Barbosa, P., Bucchignani, E., Cassano, J., Cavazos, T., Christensen, J.H., Christensen, O.B., Coppola, E., Evans, J., Geyer, B., Giorgi, F., Hadjinicolaou, P., Jacob, D., Katzfey, J., Koenigk, T., Laprise, R., Lennard, C.J., Kurnaz, M.L., Li, D., Dosio, A., 2020. Future Global Meteorological Drought Hot Spots: A Study Based on CORDEX Data. J. Clim. 33 (9), 3635–3661. https://doi.org/10.1175/JCLI-D-19-0084.1.
Spinoni, J., Barbosa, P., De Jager, A., McCormick, N., Naumann, G., Vogt, J.V., Magni, D., Masante, D., Mazzeschi, M., 2019. A new global database of meteorological drought events from 1951 to 2016. J. Hydrol.: Reg. Stud. 22. https://doi.org/10.1016/j.ejrh.2019.100593.
Spinoni, J., Naumann, G., Carrao, H., Barbosa, P., Vogt, J., 2014. World drought frequency, duration, and severity for 1951-2010. Int. J. Climatol. 34 (8), 2792–2804. https://doi.org/10.1002/joc.3875.
Stagge, J.H., Tallaksen, L.M., Gudmundsson, L., Van Loon, A.F., Stahl, K., 2015. Candidate Distributions for Climatological Drought Indices (SPI and SPEI). Int. J. Climatol. 35 (13), 4027–4040. https://doi.org/10.1002/joc.4267.
Swann, A.L.S., Hoffman, F.M., Koven, C.D., Randerson, J.T., 2016. Plant responses to increasing CO2 reduce estimates of climate impacts on drought severity. Proceedings of the National Academy of Sciences of the United States of America 113 (36), 10019–10024. https://doi.org/10.1073/pnas.1604581113.
Swart, N.C., Cole, J.N.S., Kharin, V.V., Lazare, M., Scinocca, J.F., Gillett, N.P., Anstey, J., Arora, V., Christian, J.R., Hanna, S., Jiao, Y., Lee, W.G., Majaess, F., Saenko, O.A., Seiler, C., Seinen, C., Shao, A., Sigmond, M., Solheim, L., Winter, B., 2019. The Canadian Earth System Model version 5 (CanESM5.0.3). Geosci. Model Dev. 12 (11), 4823–4873. https://doi.org/10.5194/gmd-12-4823-2019.

Tabari, H., Willems, P., 2022. Trivariate Analysis of Changes in Drought Characteristics in the CMIP6 Multimodel Ensemble at Global Warming Levels of 1.5°, 2°, and 3°C. J. Clim. 35 (18), 5823–5837. https://doi.org/10.1175/JCLI-D-21-0993.1.

Tatebe, H., Ogura, T., Nitta, T., Komuro, Y., Ogochi, K., Takemura, T., Sudo, K., Sekiguchi, M., Abe, M., Saito, F., Chikira, M., Watanabe, S., Mori, M., Hirota, N., Kawatani, Y., Mochizuki, T., Yoshimura, K., Takata, K., O'ishi, R., … Kimoto, M. (2019). Description and basic evaluation of simulated mean state, internal variability, and climate sensitivity in MIROC6. Geoscientific Model Development, 12 (7), 2727–2765. doi: 10.5194/gmd-12-2727-2019.

Taufik, M., Torfs, P.J.J.F., Uijlenhoet, R., Jones, P.D., Murdiyarso, D., Van Lanen, H.A.J., 2017. Amplification of wildfire area burnt by hydrological drought in the humid tropics. Nat. Clim. Chang. 7 (6), 428–431. https://doi.org/10.1038/nclimate3280.

Touma, D., Ashfaq, M., Nayak, M.A., Kao, S.-C., Diffenbaugh, N.S., 2015. A multi-model and multi-index evaluation of drought characteristics in the 21st century. J. Hydrol. 526, 196–207. https://doi.org/10.1016/j.jhydrol.2014.12.011.

Ukkola, A.M., De Kauwe, M.G., Roderick, M.L., Abramowitz, G., Pitman, A.J., 2020. Robust Future Changes in Meteorological Drought in CMIP6 Projections Despite Uncertainty in Precipitation. Geophys. Res. Lett. 47 (11). https://doi.org/10.1029/2020GL087820.

Ukkola, A.M., Pitman, A.J., De Kauwe, M.G., Abramowitz, G., Herger, N., Evans, J.P., Decker, M., 2018. Evaluating CMIP5 Model Agreement for Multiple Drought Metrics. J. Hydrometeorol. 19 (6), 969–988. https://doi.org/10.1175/JHM-D-17-0099.1.

Ullah, S., You, Q., Sachindra, D.A., Nowosad, M., Ullah, W., Bhatti, A.S., Jin, Z., Ali, A., 2022. Spatiotemporal changes in global aridity in terms of multiple aridity indices: An assessment based on the CRU data. Atmos. Res. 268. https://doi.org/10.1016/j.atmosres.2021.105998.

United Nations Convention to Combat Desertification, "Drought in numbers 2022: Restoration for readiness and resilience," May. 2022. https://www.unccd.int/resources/publications/drought-numbers.

van der Schrier, G., Barichivich, J., Briffa, K.R., Jones, P.D., 2013. A scPDSI-based global data set of dry and wet spells for 1901–2009. J. Geophys. Res. Atmos. 118 (10), 4025–4048. https://doi.org/10.1002/jgrd.50355.

Vicente-Serrano, S.M., Beguería, S., López-Moreno, J.I., 2010. A multiscalar drought index sensitive to global warming: The standardized precipitation evapotranspiration index. J. Clim. 23 (7), 1696–1718. https://doi.org/10.1175/2009JCLI2909.1.

Vicente-Serrano, S.M., Peña-Angulo, D., Beguería, S., Domínguez-Castro, F., Tomás-Burguera, M., Noguera, I., Gimeno-Sotelo, L., El Kenawy, A., 2022. Global drought trends and future projections. Philos. Trans. r. Soc. A Math. Phys. Eng. Sci. 380 (2238). https://doi.org/10.1098/rsta.2021.0285.

Vicente-Serrano, S. M., Quiring, S. M., Peña-Gallardo, M., Yuan, S., & Domínguez-Castro, F. (2020). A review of environmental droughts: Increased risk under global warming? In Earth-Science Reviews (Vol. 201). Elsevier B.V. doi: 10.1016/j.earscirev.2019.102953.

Wada, Y., Van Beek, L.P.H., Wanders, N., Bierkens, M.F.P., 2013. Human water consumption intensifies hydrological drought worldwide. Environ. Res. Lett. 8 (3), 34036.

Wang, T., Hamann, A., Spittlehouse, D.L., Aitken, S.N., 2006. Development of scale-free climate data for Western Canada for use in resource management. Int. J. Climatol. 26 (3), 383–397. https://doi.org/10.1002/joc.1247.

Wang, T., Tu, X., Singh, V.P., Chen, X., Lin, K., 2021. Global data assessment and analysis of drought characteristics based on CMIP6. J. Hydrol. 596. https://doi.org/10.1016/j.jhydrol.2021.126091.

Wilhite, D.A., Sivakumar, M.V.K., Pulwarty, R., 2014. Managing drought risk in a changing climate: The role of national drought policy. Weather Clim Extrem 3, 4–13. https://doi.org/10.1016/j.wace.2014.01.002.

Williams, A.P., Seager, R., Abatzoglou, J.T., Cook, B.I., Smerdon, J.E., Cook, E.R., 2015. Contribution of anthropogenic warming to California drought during 2012-2014. Geophys. Res. Lett. 42 (16), 6819–6828. https://doi.org/10.1002/2015GL064924.

Wu, F., Yang, X., Yuan, X., Ren, L., Yuan, S., Yuan, F., Jiang, S., Liu, Y., Zhang, H., 2024. How will drought evolve in global arid zones under different future emission scenarios? J. Hydrol.: Reg. Stud. 51. https://doi.org/10.1016/j.ejrh.2024.101661.

Wu, G., Chen, J., Shi, X., Kim, J.S., Xia, J., Zhang, L., 2022. Impacts of Global Climate Warming on Meteorological and Hydrological Droughts and Their Propagations. Earth's. Future 10 (3). https://doi.org/10.1029/2021EF002542.

Wu, F., Yang, X., Yuan, X., Ren, L., Yuan, S., Yuan, F., Jiang, S., Liu, Y., Zhang, H., 2024. How will drought evolve in global arid zones under different future emission scenarios? J Hydrol Reg Stud 51. https://doi.org/10.1016/j.ejrh.2024.101661.

Xu, L., Chen, N., Zhang, X., 2019. Global drought trends under 1.5 and 2 °C warming. International Journal of Climatology 39, 2375–2385. https://doi.org/10.1002/joc.5958.

Yang, Y., Guan, H., Batelaan, O., McVicar, T.R., Long, D., Piao, S., Liang, W., Liu, B., Jin, Z., Simmons, C.T., 2016. Contrasting responses of water use efficiency to drought across global terrestrial ecosystems. Sci. Rep. 6. https://doi.org/10.1038/srep23284.

Yukimoto, S., Kawai, H., Koshiro, T., Oshima, N., Yoshida, K., Urakawa, S., Tsujino, H., Deushi, M., Tanaka, T., Hosaka, M., Yabu, S., Yoshimura, H., Shindo, E., Mizuta, R., Obata, A., Adachi, Y., & Ishii, M. (2019). The Meteorological Research Institute Earth System Model Version 2.0, MRI-ESM2.0: Description and Basic Evaluation of the Physical Component. Journal of the Meteorological Society of Japan. Ser. II, 97 (5), 931–965. doi: 10.2151/jmsj.2019-051.

Zhao, T., Dai, A., 2015. The magnitude and causes of global drought changes in the twenty-first century under a low-moderate emissions scenario. J. Clim. 28 (11), 4490–4512. https://doi.org/10.1175/JCLI-D-14-00363.1.

Zhao, T., Dai, A., 2017. Uncertainties in historical changes and future projections of drought. Part II: model-simulated historical and future drought changes. Clim. Change 144 (3), 535–548. https://doi.org/10.1007/s10584-016-1742-x.

Zhao, T., Dai, A., 2022. CMIP6 Model-projected Hydroclimatic and Drought Changes and Their Causes in the 21st Century. J. Clim. 1–58. https://doi.org/10.1175/JCLI-D-21-0442.1.

Ziehn, T., Chamberlain, M.A., Law, R.M., Lenton, A., Bodman, R.W., Dix, M., Stevens, L., Wang, Y.-P., Srbinovsky, J., 2020. The Australian Earth System Model: ACCESS-ESM1.5. J. Southern Hemisphere Earth Syst. Scie. 70 (1), 193–214. https://doi.org/10.1071/ES19035.